A biophysical, minimal model to investigate age-related changes in CA1 pyramidal cell electrical activity

Erin C. McKiernan[1][*], Marco A. Herrera-Valdez[2][**], and Diano F. Marrone[3,4]

[1]Departamento de Física, Facultad de Ciencias, Universidad Nacional Autónoma de México
[2]Laboratorio de Fisiología de Sistemas, Departamento de Matemáticas, Facultad de Ciencias, Universidad Nacional Autónoma de México
[3]Department of Psychology, Wilfrid Laurier University
[4]McKnight Brain Institute, University of Arizona
[*]Corresponding author: emckiernan@ciencias.unam.mx
[**]Corresponding author: marcoh@ciencias.unam.mx

Abstract

Aging is a physiological process that is still poorly understood, especially with respect to effects on the brain. There are open questions about aging that are difficult to answer with an experimental approach. Underlying challenges include the difficulty of recording *in vivo* single cell and network activity simultaneously with submillisecond resolution, and brain compensatory mechanisms triggered by genetic, pharmacologic, or behavioral manipulations. Mathematical modeling can help address some of these questions by allowing us to fix parameters that cannot be controlled experimentally and investigate neural excitability under different conditions. Previous modeling approaches in the CA1 region of the hippocampus have provided many insights, but have also been limited by an inherent trade-off between physiological accuracy and computational load. Herein, we present a biophysical, minimal model of CA1 pyramidal cells (PCs) based on general expressions for transmembrane transport derived from basic thermodynamical principles. The model allows directly varying the contribution of transmembrane transport proteins by changing their number. By analyzing the dynamics of the model we find parameter ranges that reproduce the variability in electrical activity seen in PCs. In addition, the model explains the dynamics underlying age-related changes in excitability that are qualitatively and quantitatively similar to those observed in aging PCs as caused by increased L-type Ca^{2+} channel expression.

1   Introduction

As we age, our brains undergo many changes [1–3], but we understand relatively little about these and their effects on neural function. What does normal neurophysiological aging look like and what are the various stages? How does the electrical activity of neurons change and what are the biophysics underlying those changes? How do aging neurons respond to input from other cells? Answering these questions is not just fundamental to understanding aging as a neurophysiological process, but also to understanding how this process may be altered in age-related disorders of clinical importance such as Alzheimer's [4] and Parkinson's [5] disease.

Many aging studies have focused on the hippocampus, an area of the brain involved in learning, memory formation, and spatial processing [1–3]. Aged rats [6–11] and humans [12, 13] show impaired learning of hippocampal-dependent spatial tasks. Long-term potentiation (LTP), a proposed physiological substrate of memory formation, has been investigated in the hippocampus and its induction and maintenance shown to be impaired in aged rats [6, 10, 14, 15]. A short-term form of plasticity, frequency potentiation/facilitation (FP/FF), is also impaired in hippocampal pyramidal cells (PCs) from aged rats and correlates with learning deficits [16, 17].

Plasticity changes and behavioral impairments may result in part from altered excitability and disrupted Ca^{2+} regulation in aged neurons [1–3]. CA1 PCs from aged animals show larger and longer post-burst afterhyperpolarizations (AHPs) [18–22]. AHPs are mediated by Ca^{2+}-dependent K^+ currents, which can act like brakes on the electrical activity of CA1 PCs [23, 24]. As a result, PCs show increased spike frequency adaptation and fire fewer action potentials (APs) in response to acute stimuli or during bursting activity [25–27]. Larger AHPs are associated with increased intracellular Ca^{2+}, mediated in part by Ca^{2+} entry via L-type channels [22, 26, 28–30]. Aged animals show increases in L-type channel expression and/or channel density at the plasma membrane [31–35]. Animals with higher Ca^{2+} channel density perform poorly in spatial tasks [32], while blockers of L-type channels can restore learning and plasticity in older animals [36–38].

Despite extensive study, it is still not well understood how changes in ion channel gene expression and hippocampal PC excitability may affect neuron responsiveness and microcircuit output. In part, this is due to challenges inherent to performing the needed experiments, especially in mammalian systems. Single PCs are difficult to access in intact animals where hippocampal microcircuit function is preserved. In addition, it is difficult to tease apart the influence of each of the many different neurophysiological factors that change during aging. Mathematical modeling provides means to understand more about the effects of aging on hippocampal cellular excitability by performing manipulations that are not possible to implement in experiments.

Several mathematical models have been constructed to investigate electrical activity in CA1 PCs [39–44]. Some include representations of PC morphology using multiple compartments [41–44], making mathematical analysis difficult and increasing computational load. Single-compartment models of CA1 PCs exist, but include numerous ionic currents (up to 10) and 5 or more variables [39, 40]. As the number of variables increases, analysis becomes harder and limits our ability to understand the influence of specific parameters, as well as complicating the construction of simple network models. Finally, the existing model formulations are conductance-based (e.g. Hodgkin-Huxley type [45]), which only takes into account linear approximations of the fluxes that make up the transmembrane currents [46]. Our previous work shows that mathematical expressions

for ionic currents for different passive and active transport mechanisms can be derived from first principles of thermodynamics [46–48], using a common functional form. This results in a more realistic representation of ionic flow across the membrane, and allows the model to reproduce phenomena such as rectification of ion currents observed in recordings but not reproduced by conductance-based models.

We present a model that reproduces the diversity of firing patterns seen in CA1 PC recordings, including repetitive slow firing with frequency adaptation, stimulus-induced bursting, and sponta- neous bursting [49]. We do so by studying families of 3-dimensional dynamical systems with a common formulation (same functional form describing the dynamics), based on basic biophysical descriptions. In addition, we reproduce several electrophysiological characteristics of aging simply by varying the expression of Ca^{2+} channels in the model membrane, and make predictions about differences in bursting activity in aged cells, which to our knowledge has not yet been reported. We argue this model is ideal to further study the effects of different biophysical changes in CA1 PCs during aging, as well as potentially forming the basis for biophysical, yet computationally inexpensive network models.

2 Methods

2.1 Model

To simulate the electrical activity of CA PCs, we used an extended version of a two-dimensional, biophysical model previously developed and characterized by two of the present authors (ECM and MAHV) [46–48]. The equations for the ionic currents are derived from first principles of thermo- dynamics. The advantages of the model over conductance-based formulations include: (1) that each parameter in the model corresponds to a biophysical parameter measurable experimentaly, meaning we can easily incorporate data, as well as make testable physiological predictions; (2) our formulation allows us to vary the number of specific ion channels in the membrane explicitly (i.e., simulate functional changes in gene expression), and (3) the possibility of extensions or future studies including phenomena like rectification of ionic currents as observed in electrophysiological recordings of K^+, Cl^-, and AMPA-Kainate channels [46].

Previous modeling studies have shown that to reproduce firing behaviors such as spike frequency adaptation and bursting, the minimum number of variables is three [50, 51]. In particular, Ca^{2+} dynamics are important for producing adaptation and burst firing in CA1 PCs (for review see [49]). The model dynamics are therefore described by three ordinary differential equations for the time-dependent changes in the transmembrane potential (v, in mV), the proportion of open K^+ channels (w in [0,1]), and the intracellular Ca^{2+} concentration (c, in μM), respectively [46]. Based on a well known relationship between voltage-dependent activation of K^+delayed rectifier channels and inactivation of Na^+channels, w also represents the proportion of inactivated Na^+channels [52–54].

Explicitly, it is assumed that the membrane potential changes with the currents produced by ions transported across the membrane. In this case, we take into account currents mediated by a Na/K ATPase (I_{NaK}), voltage- and calcium-gated K^+channels (I_{DK} and I_{SK}, respectively) and a voltage-gated, inactivating Na^+channel (I_{NaT}). The time-dependent change in membrane potential

can then be written as

$$C_m \partial_t v = I_F - I_{NaT}(v, w) - I_{CaL}(v, c) - I_{DK}(v, w) - I_{SK}(v, c) - I_{NaK}(v).$$ (1)

with ∂_t representing the instantaneous change with respect to time. C_m (pF) is a constant representing the change in the density of charge around the membrane with respect to voltage, typically referred to as membrane capacitance in models based on electrical circuits [55]. Based on recordings from rat CA1 PCs, it is assumed that $C_m = 25$ pF [56].

All the currents in Eq. (1) are modeled using the same generic functional form, a product

$$I_x = a_x G_x \varphi_x,$$

$x \in \{NaT, CaL, DK, SK, NaK\}$, where a_x is a whole-cell current density (pA), G_x is a gating term (between 0 and 1), and φ_x is an adimensional term describing the driving force for the transmembrane flux (Table 1). The terms $a_x = s_x N_x$, $x \in \{NaT, CaL, DK, SK, NaK\}$ are whole cell current amplitudes with s_x (pA) representing the current flowing through a single channel (or pump), and N_x representing the number of membrane proteins mediating the current (e.g. number of K$^+$channels). Of interest, $s_x \sim 1$ pA for most voltage-gated channels [57], and it is between 5 and 10 pA for SK channels [58].

Assuming that none of the currents in the model exhibit rectification [46], the adimensional component of the transmembrane flux can be simplified and written as

$$\varphi_x(v) = 2\eta_x \sinh\left(\eta_x \frac{v - v_x}{2v_T}\right),$$ (2)

where η_x represents the number of charges transported across the membrane in a single transport event, and v_x is the reversal potential for the current, $x \in \{NaT, CaL, DK, SK, NaK\}$. For channels, v_x is the Nernst potential for the ion [46]. Of note, $\eta_x = 1$ for $x \in \{DK, SK, NaK\}$ and $\eta_{NaT} = -1$ [46], which gives

$$\varphi_x(v) = 2 \sinh\left(\frac{v - v_x}{2v_T}\right),$$

for $x \in \{NaT, DK, SK, NaK\}$. For Ca^{2+}channels, the total charge transported by one ion crossing the membrane from the extracelular space is -2, so

$$\varphi_{Ca}(v) = 4 \sinh\left(\frac{v - v_{Ca}}{v_T}\right).$$

The driving force for the flux is assumed to be the same for DK and SK channels. Therefore, the label K is used for both fluxes from here on. The thermal potential $v_T = kT/q$ (mV), where k is Boltzmann's constant (mJ/^{o}K), T is the absolute temperature (^{o}K), and q is the elementary charge (Coulombs). The Boltzmann constant can be thought of as a scaling factor between macroscopic (thermodynamic temperature) and microscopic (thermal energy) physics [59]. The reversal potentials for the different currents depend on the Nernst potentials for Na$^+$, Ca^{2+}, or K$^+$, as given by

$$v_x = \frac{v_T}{z_x} \ln\left(\frac{[x]_o}{[x]_i}\right), \quad x \in \{Na, Ca, K\}$$ (3)

where z_x is the ion valence and $[x]_o$ and $[x]_i$ are the ion concentrations outside and inside the cell, respectively. The reversal potential for the Na$^+$-K$^+$ ATPase (or pump) is given by $v_{NaK} = v_{ATP} + 3v_{Na} - 2v_K$ [46]. The Nernst potentials for K$^+$ and Na$^+$ are assumed to be constant, but v_{Ca} varies because the intracellular Ca^{2+} concentration is a state variable in the model.

Table 1: Transport mechanisms included in the model

Transport mechanism	Current	Amplitude (a)	Gating (G)	Flux φ
Transient Na$^+$ channels	$I_{NaT}(v, w)$	a_{Na}	$S_m(v)(1 - w)$	$\varphi_{Na}(v)$
L-type Ca^{2+} channels	$I_{CaL}(v, c)$	a_{Ca}	$S_n(v)$	$\varphi_{Ca}(v)$
Delayed rectifier K$^+$ channels	$I_{DK}(v, w)$	a_{DK}	w	$\varphi_K(v)$
SK Ca^{2+}-dependent K$^+$ channels	$I_{SK}(v, c)$	a_{SK}	$H_{SK}(c)$	$\varphi_K(v)$
Na$^+$-K$^+$ pumps	$I_{NaK}(v)$	a_{NaK}	1	$\varphi_{NaK}(v)$

All ion fluxes are given by a product of the form $I_x = a_x G_x \varphi_x$ where a_x, G_x, and φ_x represent, respectively, the amplitude (normalized by membrane capacitance), gating, and driving force terms for the flux. $G_{NaK} = 1$ to represent saturation of the Na$^+$-K$^+$ pumps. Note that the inactivation of Na$^+$-channels is also represented by w [53, 54]. The proportion of non-inactivated Na$^+$ channels is thus $1 - w$.

Gating.   The auxiliary functions describing voltage-dependent activation are given by

$$S_j(v) = \frac{\exp\left(g_j \frac{v - v_j}{v_T}\right)}{1 + \exp\left(g_j \frac{v - v_j}{v_T}\right)}, \quad j \in \{m, n, w\}, \tag{4}$$

where g_j represents the steepness of the activation curve for Na$^+$(m), Ca^{2+}(n), or DK (w) channels; v_j represents the half-activation voltage for those channels. The function

$$R_w(v) = r_w \left[\exp\left(b_w g_w \frac{v - v_w}{v_T}\right) + \exp\left((b_w - 1)g_w \frac{v - v_w}{v_T}\right)\right], \tag{5}$$

describes the voltage-dependence of the rate of activation of the DK channels. The parameters r_w and b_w represent the recovery rate and the asymmetry in the gating relative to voltage that biases the time constant for the gating process, respectively.

The dynamics for the proportion of activated DK channels, w, are assumed to be logistic,

$$\partial_t w = w(S_w(v) - w)R_w(v), \tag{6}$$

which yields better fits and is more consistent with the dynamics of activation in channel populations recorded in voltage-clamp experiments [45, 60, 61].

The gating of the SK channel is not voltage-dependent, but instead depends on intracellular Ca^{2+}- binding. Its activation is modeled using a Hill equation that depends on the intracellular

concentration of Ca^{2+}, as used to fit data from channel recordings [62]:

$$H_{SK}(c) = \frac{c^2}{c^2 + c_{SK}^2},$$ (7)

where c_{SK} represents the half-activation Ca^{2+} concentration for the SK channels, with a reported value of $0.74\mu M$ (740nM) [58, 63].

For the dynamics of intracellular Ca^{2+}, we assume recovery toward a steady state c_∞ at a rate r_c, with increments caused by the Ca^{2+} current I_{Ca} [54],

$$\partial_t c = r_c(c_\infty - c) - \tilde{k}_c I_{CaL}(v, c).$$ (8)

The term $\tilde{k}_c$ in equation (8) is a conversion factor (μ M/pCoul) that accounts for the effect of Ca^{2+} flux across the membrane on the intracellular Ca^{2+} concentration.

The term I_F represents a stimulus *forcing* the membrane; that is, current from an electrode, or time-dependent fluctuations from the local field potential. Spontaneous activity is simulated by replacing the term I_F with a time-dependent, Ornstein-Uhlenbeck (OU) process with amplitude $a_F(t)$ (pA). The mean is represented by μ_F (pA) (drift term) [64] given by [65, 66]

$$a_F(t + \delta) = a_F(t)\left(1 - \frac{\delta}{\tau_F}\right) + \left[\mu_F\delta + \eta(t)\sqrt{d_{Stim}\delta}\right],$$ (9)

where δ is a small time step, τ_F is a relaxation time, $\eta(t)$ is an independent white noise process with zero-mean and unit standard deviation. The process has a variance $\sigma_F^2 = d_F\delta/2$ (pA), which means d_F can be approximated if an estimation of the variance of the current a_F is available [67, 68].

Change of variables to obtain numerical solutions. To simplify the numerics, we change variables

$$u = v/v_T,$$

and adjust all voltages accordingly as

$$u_l = v_l/v_T, \quad l \in \{NaT, CaL, K, NaK, m, n, w\}.$$

The new equation for the normalized voltage is

$$\partial_t u = \frac{\partial_t v}{v_T}.$$

To simplify the notation and reduce the number of operations during the numerical integration, we also reparametrize the amplitudes as

$$A_l = \frac{2a_l|\eta_l|}{v_T\,Cm},$$ (10)

for $l \in \{NaT, CaL, K, NaK\}$, in units of 1/ms. Similarly, the activation functions for the NaT, CaL, and DK currents can also be rewritten respectively as

$$f_\infty(u) = \{1 + \exp[g_f(u_f - u)]\}^{-1}, \quad f \in \{m, n, w\}.$$ (11)

The result is a new equation of the form

$$\partial_t u = J_F - A_{NaT}(1-w)m_\infty(u)\varphi_{Na}(u) - A_{CaL}n_\infty(u)\varphi_{Ca}(u,c) -$$

$$\left(A_{DK}w + A_{SK}H_{SK}(c)\right)\varphi_K(u) - A_{NaK}\varphi_{NaK}(u). \tag{12}$$

The term J_F (1/ms) is the input current I_F (pA) divided by $v_T C_m$. After the change in variables and the normalization of the current amplitudes, equation (8) changes to

$$\partial_t c = r_c(c_\infty - c) - k_c A_{CaL}n_\infty(u)\varphi_{Ca}(u,c), \tag{13}$$

where $k_c = \tilde{k}_c v_T C_m$.

2.2 Parameters

The currents were modeled to fit as closely as possible the biophysical properties of those carried by channel variants expressed in mammalian neurons, and specifically CA1 PCs, where data are available. For example, the DK current is based on that mediated by $K_v2.1$ channels, found to be the predominant channel underlying the delayed rectifier current in rat hippocampal neurons [69]. The L-type Ca^{2+} current is based on that carried by $Ca_v1.2$ (class C) channels, found to be the predominant L-type channel isoform expressed in rat brain [70]. Additional details about the model current parameters can be found in Table 2.

Wherever possible, model parameters were taken from studies in rodent (mice and rat) hippocampal CA1 PCs. If data were not available, we obtained parameters from other types of mammalian cell, or from studies of mammalian ion channels in expression systems like *Xenopus* oocyte. Physical constants and other parameters which we would not expect to vary, such as the intra- and extracellular concentrations of ions or the cellular capacitance, were fixed. Biophysical properties of the ion channels, such as their half-activation voltages, were also fixed. The parameters we varied were primarily those corresponding to maximum current amplitudes, which can change acutely due to modulation or channel phosphorylation [71, 72], or chronically due to changes in ion channel expression that occur with age [31, 33, 73].

Table 2: Constants and parameters

parameter	description	value	units	reference
k	Boltzmann's constant	1.381e^{-20}	mJ/K	physical constant [57]
q	elementary charge	1.602e^{-19}	C	physical constant [57]
T	absolute temperature	273.15 + 37	K	adjusted to mammalian body temperature of 37 °C [57]
a_{NaT}	amplitude of transient Na$^+$ current	1000-2300	pA	set to produce currents of ∼2-7 nA, in the range recorded in CA1 PCs from rats [74] and guinea pigs [75]
a_{CaL}	amplitude of L-type Ca^{2+} current	25 or 50	pA	set to produce currents of ∼2-3 nA or ∼5-6 nA as recorded in young and aged CA1 PCs, respectively [28]

parameter	description	value	units	reference
a_{DK}	amplitude of delayed rectifier K$^+$ current	6000-8000	pA	set to produce currents of $\sim$6-9 nA, in the range recorded from HEK cells expressing rat Kv2.1 and I_K in hippocampal neurons [76]
a_{SK}	amplitude of Ca^{2+}-dependent K$^+$ current	300-1600	pA	set to produce currents of $\sim$100-800 pA, depending on Ca^{2+} concentration, as recorded in SK-transfected cells [77]
a_{NaK}	amplitude of Na$^+$/K$^+$ ATPase current	10-23	pA	set to produce currents of $\sim$?-? pA, similar to but on high end of range recorded in hippocampal PCs [78]
η_x	charge moved across the membrane in a single transport event $x \in \{NaK, DK, SK\}$	1	–	1 net positive charge moving outward [46]
η_{NaT}	charge transported across the membrane by NaT channels	-1	–	1 net positive charge moving inward [46]
η_{CaL}	charge transported across the membrane by Ca channels	-2	–	2 net positive charges moving inward [46]
v_{Na}	Nernst potential for Na$^+$	60	mV	in range reported for mammalian cells [79]
v_{Ca}	Nernst potential for Ca^{2+}	variable; baseline $\sim$128	mV	in range reported for mammalian cells [79]; varies since intracellular Ca^{2+} concentration is a model variable
v_K	Nernst potential for K$^+$	-89	mV	in range reported for mammalian cells [79]
v_{ATP}	Nernst potential for ATP	-420	mV	value used in model of mammalian heart cells and based on fit to data [80]
v_{NaK}	Nernst potential for Na$^+$/K$^+$ ATPase	-62	mV	calculated based on the Nernst potentials for ATP, Na$^+$, and K$^+$, and a 3:2 stoichiometry, respectively [81]; $v_{NaK} = 3v_{Na} - 2v_K - v_{ATP}$
r_w	rate of activation of delayed rectifier K$^+$ current	1.0-1.8	ms	fit so that the duration of the action potential is approximately 2 milliseconds [82]
s_w	symmetry of time constant of delayed rectifier K$^+$ current	0.3	-	based on fit; if higher (0.5-0.7) APs are the wrong shape and do not ride on sufficient plateau potential compared to recordings
v_m	half-activation potential of Na$^+$ current	-19	mV	in range reported for transient Na$^+$ channels in CA1 PCs [83–85]

parameter	description	value	units	reference
v_n	half-activation potential of Ca^{2+} current	3	mV	in range recorded for high-voltage activated Ca^{2+} currents in rat CA1 PCs [86]; see also recordings from oocytes [87] or HEK cells [88] expressing $Ca_v1.2$ channels
v_w	half-activation potential of delayed rectifier K^+ current	-1	mV	in range reported for rat Kv2.1 channels expressed in COS-1 cells [69]
c_{SK}	half-activation Ca^{2+} concentration for SK current	740	nM	based on recordings from oocytes expressing rat SK channel variant [58, 63]
g_m	activation slope of Na^+ current	5.0	-	in range reported for Na^+ current in mouse [89] and rat [90] CA1 neurons
g_n	activation slope of Ca^{2+} current	5.0	-	
g_w	activation slope of delayed rectifier K^+ current	3.8	-	fit to data from rat brain delayed rectifier channels [91]
c_∞	minimum intracellular Ca^{2+} concentration	100	nM	approximate resting intracellular Ca^{2+} concentration in rat CA1 PCs [25, 92, 93]
r_c	intracellular Ca^{2+} removal rate constant	$1e^{-3}$ to $5e^{-3}$	ms^{-1}	adjusted to produce Ca^{2+} dynamics as recorded in rat CA1 PCs [92]
k_c	conversion factor to calculate effect of Ca^{2+} current on intracellular Ca^{2+} concentration	$3e^{-6}$ to $6e^{-6}$	nM/pCoul	adjusted to produce Ca^{2+} dynamics as recorded in rat CA1 PCs [92]

By exploring the model through parameter variations, we were able to find parameter sets that produced different firing patterns, such as adaptive firing, conditional bursting, and spontaneous bursting. These firing patterns are described in more detail in the Results section, but the respective parameter sets are included in Table 3 for ease of comparison.

2.3   Simulations

All code was written in Python 3.7.4 and run on MacBook Pro laptops with 2.9 GHz Intel Core i5 processors. Simulations were performed using functions from the Python library NumPy [94]. Figures were produced with the Python library Matplotlib [95]. OU processes were simulated using the pyprocess (pypi.org/project/pyprocess) module [96].

Table 3: Parameters used to produce different firing patterns in the young PC model. See equation (10).

parameter	adaptive firing	conditional bursting	spontaneous bursting
a_{NaT} (A_{NaT})	1000 (2.99)	1300 (3.89)	2300 (6.88)
a_{CaL} (A_{CaL})	25 (0.15)	25 (0.15)	25 (0.15)
a_{DK} (A_{KD})	8000 (23.95)	6000 (17.96)	7000 (20.95)
a_{SK} (A_{SK})	1400 (4.19)	1600 (4.79)	300 (0.90)
a_{NaK} (A_{NaK})	10.0 (0.03)	13 (0.04)	23 (0.07)
r_w	1.0	1.8	1.1
r_c	$1e^{-3}$	$5e^{-3}$	$5e^{-3}$
k_c	$3e^{-6}$	$6e^{-6}$	$6e^{-6}$

Original amplitudes (a_x) are in pA. Reparametrized amplitudes (A_x) in parentheses are calculated by $2 * \frac{a_x}{v_T C_m}$ for $x \in \{NaT, DK, SK, NaK\}$ and $4 * \frac{a_{CaL}}{v_T C_m}$ for Ca^{2+} channels. For all calculations, $v_T C_m$ = 668.171 mv pF.

2.4   Code availability

All Python code from this study is available via GitHub (github.com/emckiernan/agingCA1) and shared under the MIT license (opensource.org/licenses/MIT) to facilitate reuse. To promote reproducibility, code is embedded in a Jupyter notebook [97, 98] that explains how to use the code and generate the figures presented here.

2.5   Study design

While aged cells display a number of biophysical changes, we focused on their Ca^{2+} channel expression. Aged CA1 PCs show an increase in the number of functional transmembrane L-type Ca^{2+} channels [31–34, 99]. In particular, CA1 PCs from aged rats have increased expression of $Ca_v 1.2$ at the plasma membrane [35]. With these results in mind, we decided to simulate one aspect of aging by changing the number of $Ca_v 1.2$ channels in our model membrane. We asked the question, is a change in $Ca_v 1.2$ expression sufficient to reproduce the various changes in excitability, such as increased spike frequency adaptation, observed experimentally in aged CA1 PCs? In addition, CA1 PCs are known to burst [49], but we are not aware of any studies comparing the bursting patterns of young versus aged animal cells. Therefore, we used our model to further investigate the effects of altered $Ca_v 1.2$ channel density on bursting activity. The PC models for young and old animals will be referred to as yPC and aPC, respectively. In all the following simulations, yPCs and aPCs are identical with respect to every parameter except the maximum amplitude of their L-type Ca^{2+} current, which is set to produce currents of ~2-3nA or ~5-6nA to match the magnitude of currents seen in recordings from young and aged animal CA1 PCs, respectively [28].

3 Results

CA1 PCs display diverse firing patterns, ranging from repetitive spiking with frequency adaptation to stimulus-induced, or even spontaneous, bursting (for review see [49]). Thus, to accurately represent these cells, our model must reproduce this diversity of firing as well as age-related effects on firing already reported in the literature.

3.1 Modeling age-related changes in spike frequency adaptation

Many CA1 PCs respond to square-pulse current injection by firing several early spikes followed by adaptation which slows the frequency of firing [25, 100–106]. Therefore, our first challenge was to tune the model to produce an adaptive firing pattern. We set the ionic currents to be the same amplitude range as observed in patch recordings of young adult CA1 PCs, with amplitudes for the Na^+ and Ca^{2+} currents at $\sim$2-3 nA, the DK current approximately double the inward cationic currents, and the SK current at $\sim$400-700 pA, depending on the intracellular Ca^{2+} concentration (see Table 2 for more details and references). This balance of ionic currents successfully generates adaptive firing similar to recordings (Fig. 1A, left column).

Studies show that adaptation is more pronounced in aged than in young animals, leading to a shorter initial period of fast spiking, followed by fewer spikes or even complete cessation of firing [25–27, 107]. Stronger adaptation in PCs from aged animals may be relevant to circuit function, as it is correlated with learning impairment [27, 107]. To compare the yPC and aPC models, all parameters were fixed except for the maximum amplitude of the L-type Ca^{2+} current, which was set to produce currents of $\sim$2-3 nA (young) or $\sim$5-6 nA (old), based on recordings [28]. Increased Ca^{2+} channel density in the aPC model causes the number of spikes fired in the first $\sim$100 ms after stimulus onset to decrease from 6 to 4 spikes, and further slows firing for the remaining period of current injection (Fig. 1A, right column). These results are similar to those found in recordings of CA1 PCs in young and old rabbits [26].

Comparing the ionic currents produced in each PC model during individual APs (Fig. 1B), we see that the Na^+ currents are equivalent in the two cells but the Ca^{2+} current in the aPC is approximately double that in the yPC, as expected with our parameter settings. Interestingly, despite setting the DK channel amplitude to be the same in the two cells, I_{DK} was larger in the aPC by $\sim$2 nA. This increased I_{DK} appears to be a consequence of the larger depolarization produced in the aPC model due to increased Ca^{2+} influx. The APs in the aPC are a few millivolts larger than those in the yPC, which increases the driving force for K^+ entry. However, increased I_{DK} is not responsible for the stronger adaptation in the aPC, as this current decreases rather than increases as firing proceeds. Furthermore, scaling I_{DK} back down in the aPC to compensate does not recover the firing pattern seen in yPCs. These results are not shown here, but can be confirmed by running the corresponding simulations in our Jupyter notebook (found at github.com/emckiernan/agingCA1).

Examining the voltage response and the Ca^{2+} and SK currents generated in the first 120 ms after stimulus onset reveals the mechanisms underlying the stronger adaptation in the aPC model (Fig. 2). The large Ca^{2+} current causes the aPC to fire soon after stimulus onset. However, over time, the larger increase in intracellular Ca^{2+} in turn produces a larger SK current, which slows firing to a greater extent in the aPC. While the first two spikes occur nearly simultaneously in the aPC
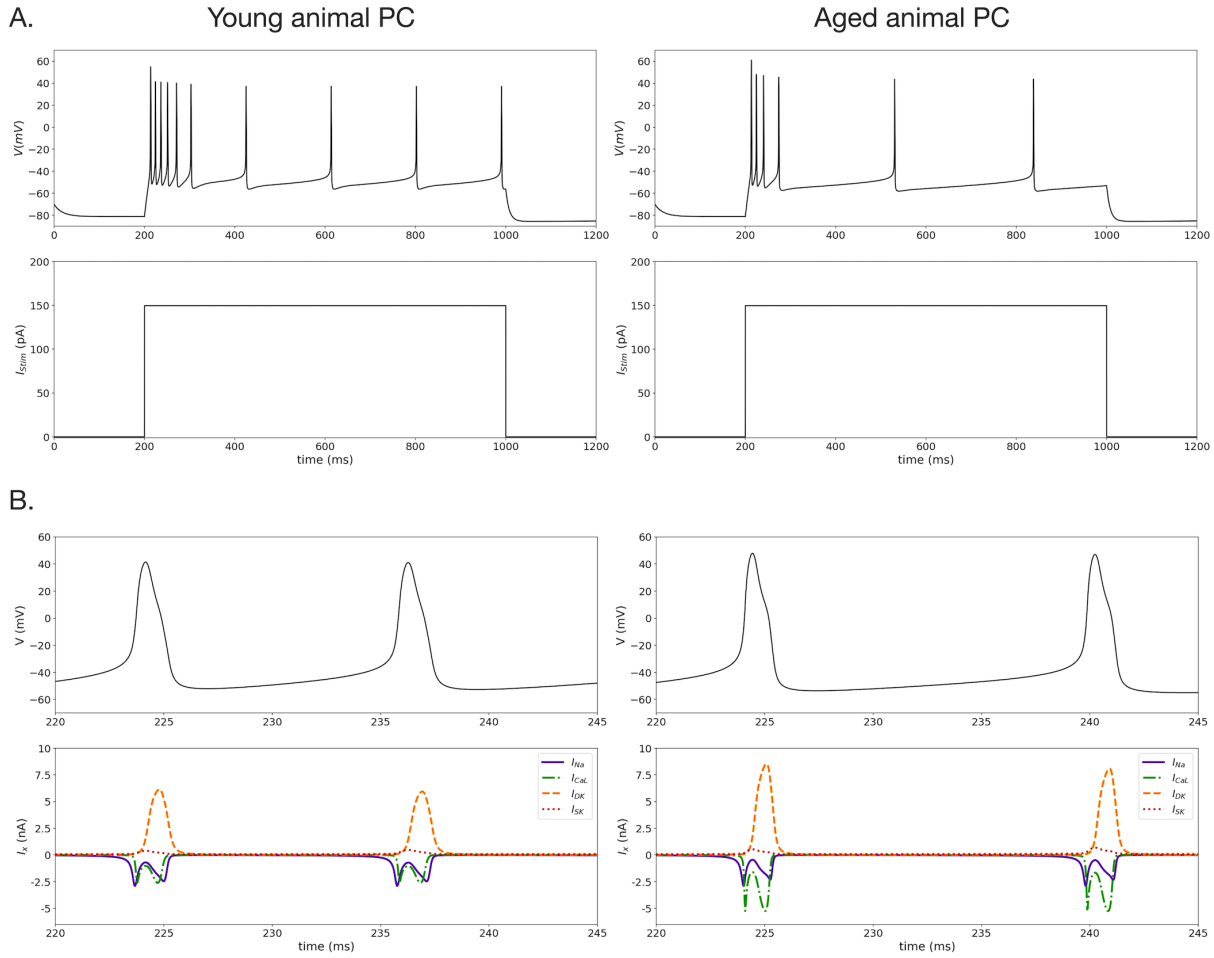
Figure 1: Responses of yPC (left column) and aPC (right column) models to an 800 ms 150 pA square pulse current injection. **A.** Top row shows the voltage responses of each cell to the stimulus shown in the second row. **B.** Zoom-in on two APs fired early in the response to better visualize their time course and amplitude, while below shows the amplitude and dynamics of the corresponding ionic currents. Parameters for yPC: a_{NaT} = 1000, a_{CaL} = 25, a_{DK} = 8000, a_{SK} = 1400, r_w = 1.0, r_c = 1e^{-3}, and k_c=3e^{-6}. All parameters for aPC the same except a_{CaL}=50. Units for all parameters can be found in Table 2.

and yPC, by the third spike the aPC falls behind and the yPC spikes sooner. By the fourth spike, activity in the aPC is significantly delayed with respect to the yPC. The aPC fails to spike again in this time period, while the yPC fires again. Closer inspection of the voltage traces, especially following the fourth aPC spike, shows a prolonged AHP that prevents the cell from firing.

3.2 Modeling age-related changes in AHPs

AHP generation has been studied in CA1 PCs [41, 108, 109], particularly in the context of aging and excitability [21, 22, 25, 26, 107, 110–113]. To induce AHPs, we kept the same parameters as in the previous simulations. We then stimulated model neurons with a 100 ms square pulse of sufficient amplitude to generate a burst of 4 APs (Fig. 3). The AHPs produced under these conditions in the
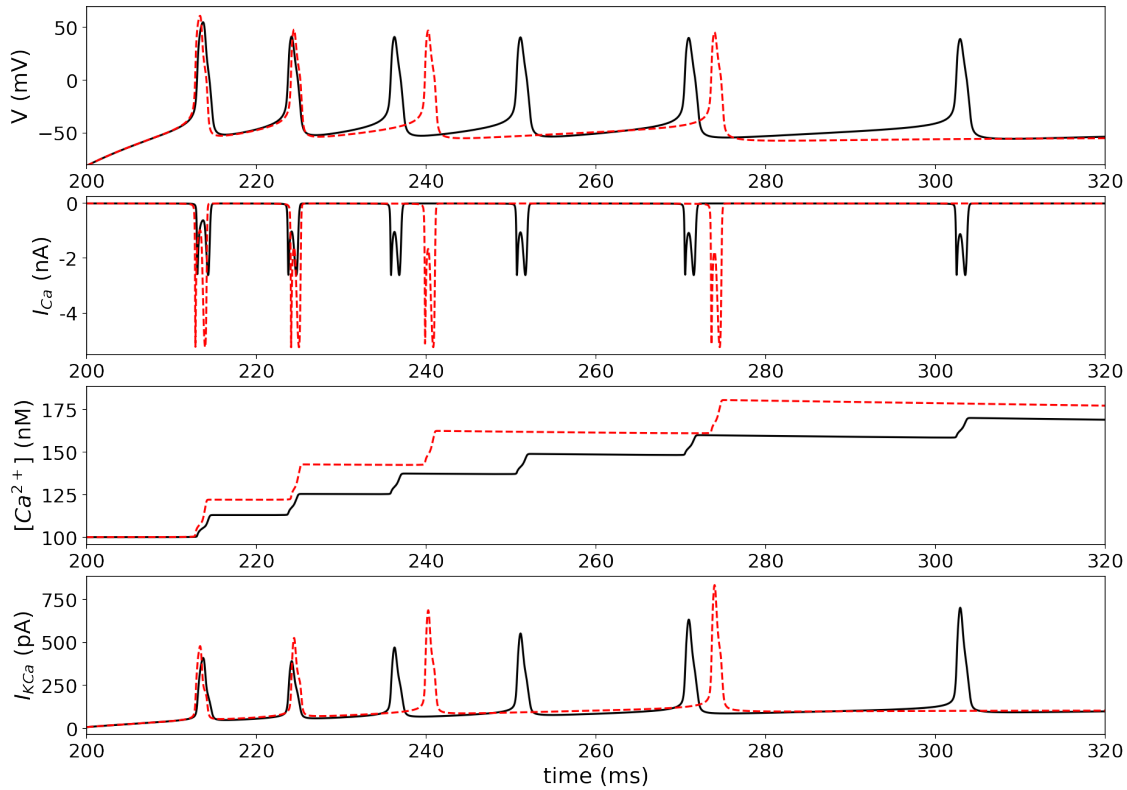
Figure 2: Spike frequency adaptation in the yPC (solid black traces) versus aPC (dashed red traces) models. First 120 ms of voltage responses (top panel) shown in Fig. 1. Corresponding Ca^{2+} currents, intracellular Ca^{2+} concentration, and SK currents for each cell can be seen in the second, third, and fourth rows, respectively.

yPC model had a peak amplitude of ∼4 mV, similar to recordings [22, 113, 114].

The aPC model required more current than the yPC model to fire the same number of spikes (112 vs. 142 pA), suggesting that the aPC model is less excitable. However, the aPC fires earlier than the yPC due to its increased Ca^{2+} current (Fig. 3, top panel inset). The aPC generates an AHP ∼1-2 mV larger than seen in the yPC (Fig. 3, second panel), similar to the magnitude of the difference observed in recordings [22, 25, 26, 111]. In the model, this larger AHP is due to an increased accumulation of Ca^{2+} in the aPC, which in turn produces a larger SK current (Fig. 3, third and fourth panels).

3.3   Modeling age-related changes in burst firing

3.3.1   Bursting in response to stimulation

Some CA1 PCs fire bursts instead of trains of individual spikes, [40, 115–117], especially in certain developmental periods [118]. Burst firing can be generated in the model with several different parameter combinations. For the following simulations, we increased the amplitude of the Na^+ current, decreased the amplitude of the DK current and increased its activation time constant, increased the amplitude of the SK current, and made changes to the Ca^{2+} handling, all within
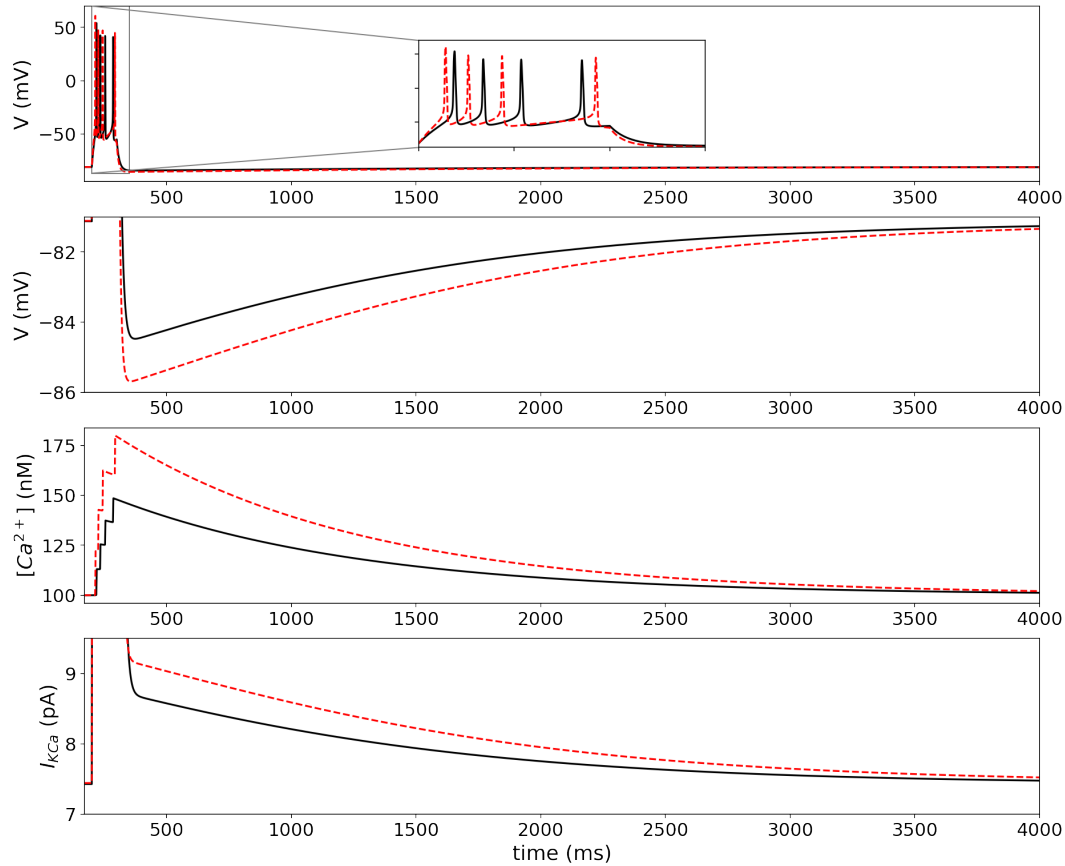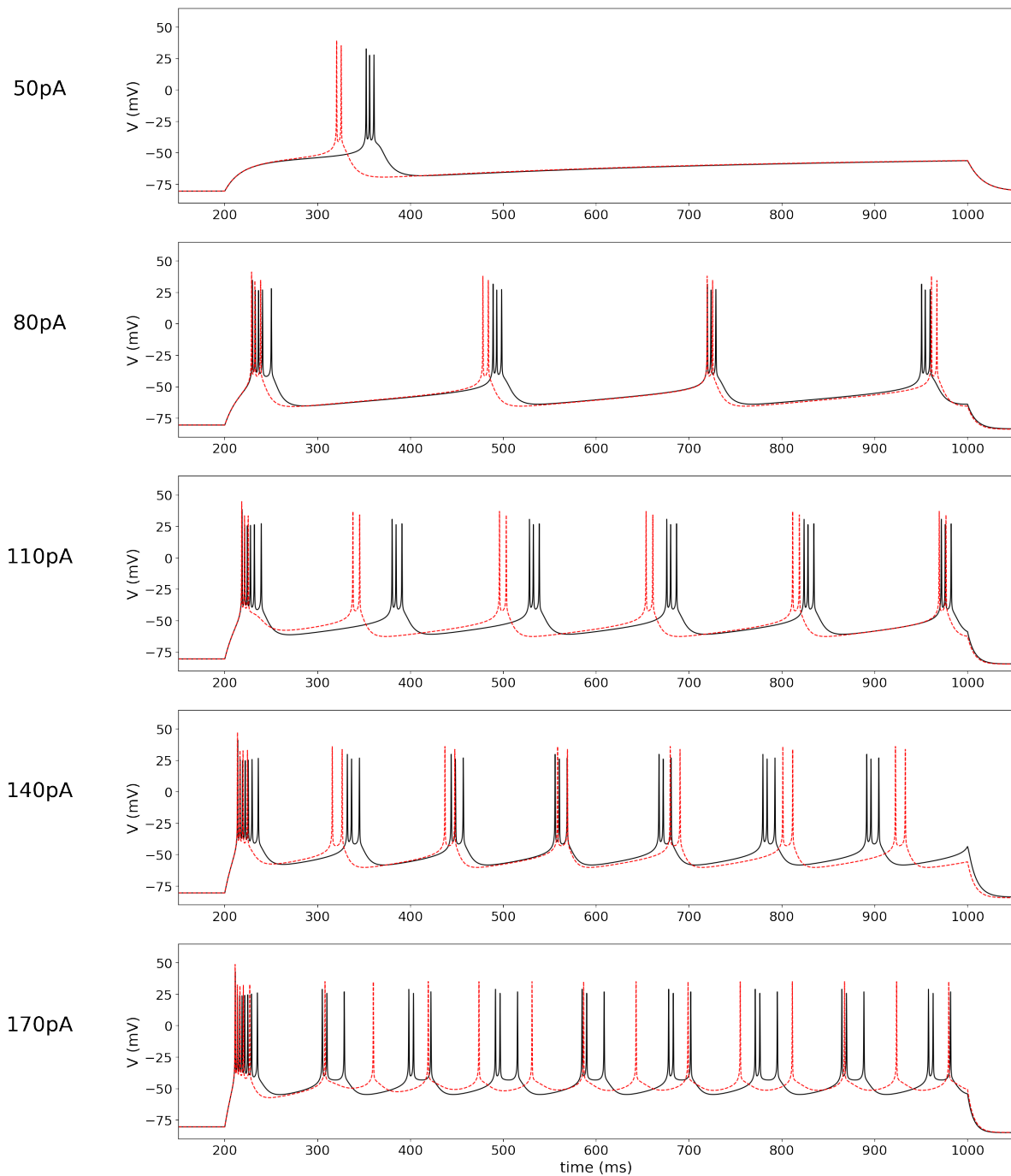
Figure 3: Responses of the yPC (solid black traces) and aPC (dashed red traces) models to 100 ms pulse (top panel). Current amplitude adjusted to produce 4 spikes in each cell (yPC: 112 pA; aPC: 142 pA). Inset zooms in to see the temporal relationship of spiking in the two cells. Second panel zooms in to better show the amplitude and time course of the AHP. The intracellular Ca^{2+} concentration and SK currents for each cell can be seen in the third and fourth panels, respectively. Same parameters as previously.

physiological limits. Under this parameter regime, model PCs are silent at rest but burst if stimulated (Fig. 4).

To explore the effects of aging on bursting, we fixed all parameters except for the maximum Ca^{2+} current amplitude, as in previous simulations. We then stimulated the two model PCs with a series of square pulse current injections ranging from 50 to 170 pA in steps of 30 pA to compare their responses. As mentioned previously, the larger Ca^{2+} current in the aPC model causes it to fire either sooner or nearly simultaneously with the yPC shortly after stimulus onset in all simulations. However, the relative timing of the two PCs' firing after the first burst depends on the stimulus amplitude (Fig. 4).

At 50 pA, the aPC model bursts sooner but fires fewer spikes per burst than the yPC model. At 80 pA, the initial bursts of the two PCs are nearly coincident, and the cells continue to fire almost at the same time, with only slight differences in burst times. At 110 pA, the two PCs again fire nearly simultaneously at the onset. However, because the aPC fires fewer spikes per burst, it is able to recover sooner and burst before the yPC for several cycles. It is only towards the end of the

Figure 4: Bursting in the yPC (solid black traces) and aPC (dashed red traces) models in response to 800 ms current injections of varying stimulus amplitudes (indicated to the left of each panel). Parameters for yPC: a_{NaT} = 1300, a_{CaL} = 25, a_{DK} = 6000.0, a_{SK} = 1600, r_w = 1.8, r_c = 5e^{-3}, k_c = 6e^{-6}. All parameters for aPC the same except a_{CaL} = 50.

268 stimulus that the larger AHP in the aPC eventually brings it into sync again with the yPC. At 140
269 pA, both PCs show stronger adaptation, with the time between the spikes in their bursts increasing.
270 The two PCs maintain similar burst timing until the last few cycles, when the aPC falls behind the

271 yPC. Finally, at 170 pA, the interspike interval in the aPC becomes so large that it spikes tonically
272 rather than bursting, while the yPC continues to fire what could be seen as bursts, though with a
273 delayed third spike in each. Depending on what we consider the relevant electrical event – the
274 single spike or the burst – the aPC shows an increased number of events relative to the yPC, but
275 the normal bursting pattern is lost.

276 3.3.2 Spontaneous bursting

277 A small percentage of CA1 PCs fire spontaneous bursts in the absence of stimulation [116, 117,
278 119]. To generate spontaneous bursting in model neurons, we increased the amplitude of both the
279 Na$^+$ and DK currents, decreased the time constant of activation for the DK current, and decreased
280 the amplitude of the SK current. Under this parameter regime, the yPC model fires spontaneous
281 bursts at a frequency of $\sim$1 Hz with 3 spikes per burst (Fig. 5), similar to recordings [40].
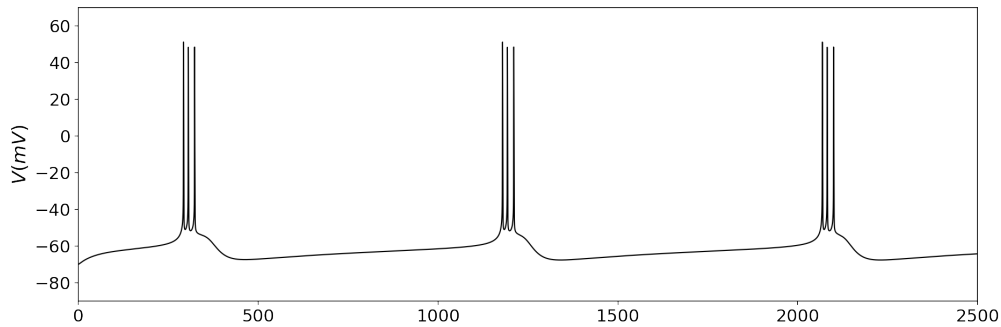

Figure 5: Spontaneous bursting in the yPC model. Parameters: a_{NaT} = 2300, a_{CaL} = 25, A_{DK} = 7000, a_{SK} = 300, r_w = 1.1, r_c = 5e^{-2}, k_c = 6e^{-6}, I_F = 0.0.

282 Increasing the Ca^{2+} channel density to simulate aging, as previously, change the spontaneous
283 firing pattern (Fig. 6). Additional interesting effects can be seen if we vary the DK current amplitude
284 within the range previously used for simulations, 6000-8000 pA (6-8 nA) in steps of 500 pA. At the
285 highest level of DK current amplitude (8 nA), the yPC continues to burst spontaneously, as seen in
286 Fig. 5, at a frequency of $\sim$1Hz but with only 2 spikes per burst. The aPC, on the other hand does
287 not burst, but rather spikes tonically at a frequency of $\sim$2Hz. When the DK current amplitude is
288 reduced (7.5 nA), the yPC continues to burst, now with 3 spikes per burst, while the aPC continues
289 to spike tonically.

290 Reducing the DK amplitude further (7 nA), now causes both PCs to burst spontaneously, though
291 the aPC fires only 2 versus 3 spikes per burst. While the Ca^{2+} current is larger for the aPC model,
292 the maximum accumulation of Ca^{2+} is only $\sim$10-15 nM more than in the yPC. There is a larger SK
293 current in aPC due to the increased Ca^{2+}, but again, because the yPC fires an additional time, the
294 two cells end up reaching nearly the same maximum current amplitude (only a $\sim$15 pA difference).
295 In other words, the 'brake' on the two cells is almost equal, and the larger Ca^{2+} influx in the aPC
296 model then means that it can burst at a slightly higher frequency.

297 Decreasing the DK amplitude still further (6.5 nA), removes some of the 'brake' on the yPC and
298 causes it to increase the number of spikes per burst to 5, while the aPC remains at 2 spikes per
299 burst. This increased spiking causes the Ca^{2+} accumulation per burst to now be larger in the yPC,
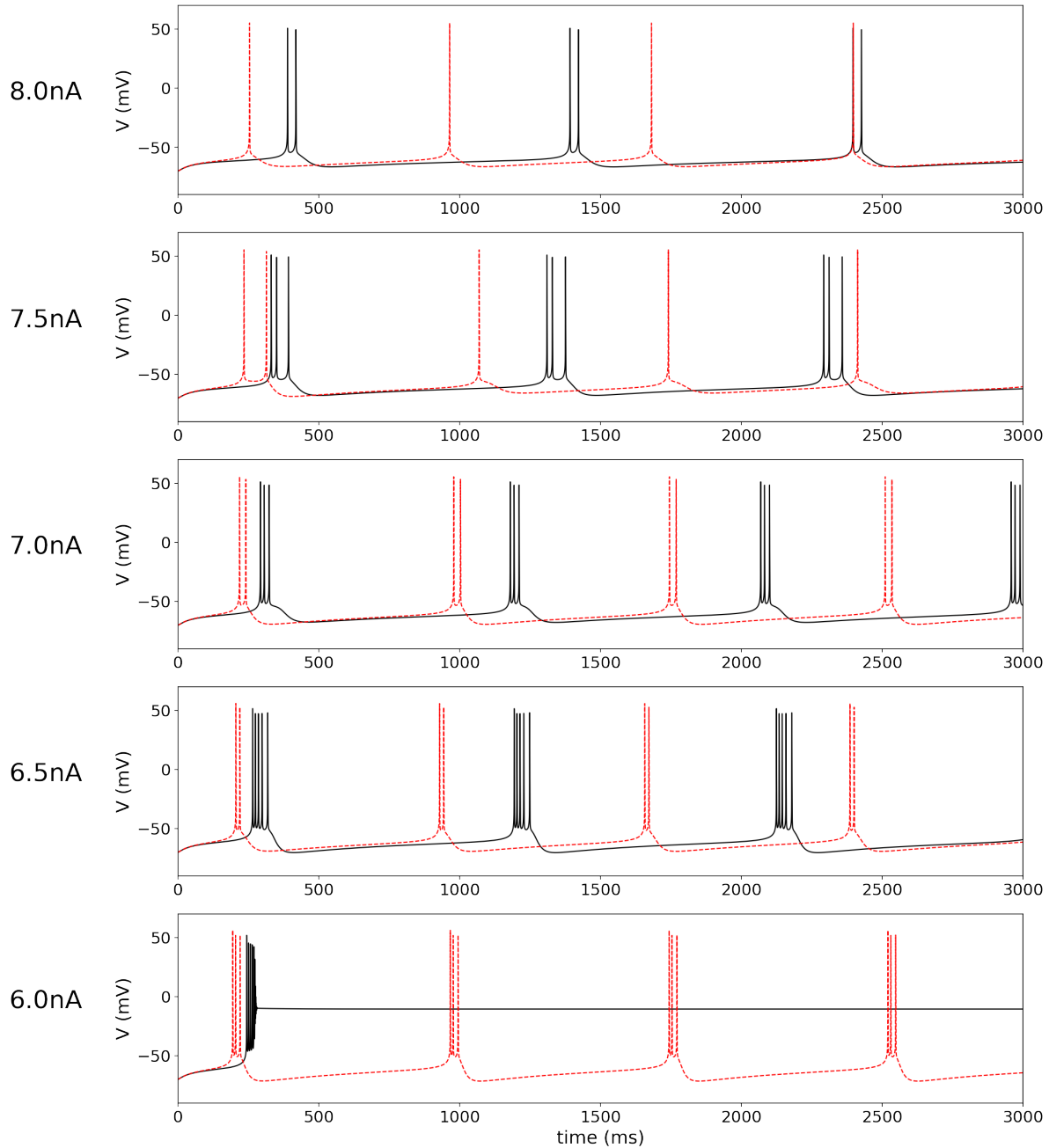
Figure 6: Comparison of spontaneous electrical activity in the yPC (solid black traces) and aPC (dashed red traces) for different levels of DK current amplitude. a_{DK} decreasing from 8000 to 6000 pA (8 to 6 nA) in steps of 500 pA, as indicated. Other parameters for yPC the same as in Fig. 5. All parameters for aPC the same except $a_{CaL} = 50$.

despite its lower amplitude setting, relative to the aPC. In turn, the yPC experiences a larger SK current and bursts one less time than the aPC. Finally, reducing the DK amplitude to its lowest level (6.0 nA), removes the remaining 'brake' on the yPC and causes it to spike at high frequency and then quickly become block depolarized. The aPC, on the other hand, retains the normal spontaneous burstng pattern, now with 3 spikes per burst. These results illustrate the importance

of the balance between the different ionic currents, and have interesting implications for our thinking regarding aged PC excitability (see Discussion).

3.4   Responses to local field potential forcing

Square pulse stimulation is useful and crucial for examining the timing of neural responses and also to calibrate the model so that the different currents yield responses like those observed experimentally. However, square pulse stimulation is not a physiologically realistic stimulus. Instead, to simulate local field potential (LFP) forcing onto CA1 PCs, we use an Ornstein-Uhlenbeck stochastic process [67, 68], as in Eq. 9. We began by stimulating model PCs with parameters set to produce an adaptive firing pattern, as in Section 3.1. In the yPC model, LFP forcing produced repetitive, irregular firing at a frequency of ∼3Hz on average (Fig. 7, top panel). This firing pattern and frequency is similar to recordings of spontaneous firing in CA1 PCs [120, 121], particularly in response to specific brain rhythms recorded in the surrounding field [122–124].

The aPC model with increased Ca^{2+} channel expression show a similar irregular firing pattern, but with a slower frequency (Fig. 7, second panel; also compare overlap in third panel). In a time window of 4 seconds, the yPC model fires 14 times, while the aPC fires only 9 times. In fact, the simulation shows several time points when the two cells fire almost simultaneously and then the yPC model fires again while the aPC fails to do so. This apparent 'spike failure' has been observed in recordings of PCs from aged animals [21].

Next, we set the parameters to produce conditional bursting, as previously.[1] Under these conditions, LFP forcing in the yPC model produced irregular burst firing at a frequency of ∼4Hz (i.e., low end of theta frequency) with a variable number of spikes per burst (Fig. 8, top panel). This firing pattern is similar to spontaneous activity recorded in a subset of CA1 PCs known as phasic theta-ON cells, which preferentially burst during theta activity recorded from the surrounding field [122, 123, 125]. Increasing Ca^{2+} channel expression in the aPC model changes the firing pattern (Fig. 8, middle panel). In response to LFP forcing, the aPC still fires irregular bursts, but with fewer spikes per burst and a higher occurrence of 2-spike bursts than seen in the yPC. In addition, the aPC fires single APs amidst the bursts, which is not seen in the yPC under this parameter regime. Also, the timing of the bursts in the aPC model is altered relative to the yPC model (see third panel overlap).

4   Discussion

4.1   Cellular heterogeneity

Here we show that a three-dimensional, single-compartment model derived from first principles of thermodynamics is capable of reproducing the diversity of firing patterns recorded in CA1 PCs. Moving between the different adaptive and bursting firing patterns was achieved primarily by changes to the relative expression of ion channels in the model. While we did not systematically explore the full parameter space, future work could include bifurcation analysis to determine the

---

[1]We also stimulated model PCs with LFP forcing when parameters were set to produce spontaneous bursting. This result is not shown here but can be explored in our Jupyter notebook (found at github.com/emckiernan/agingCA1).
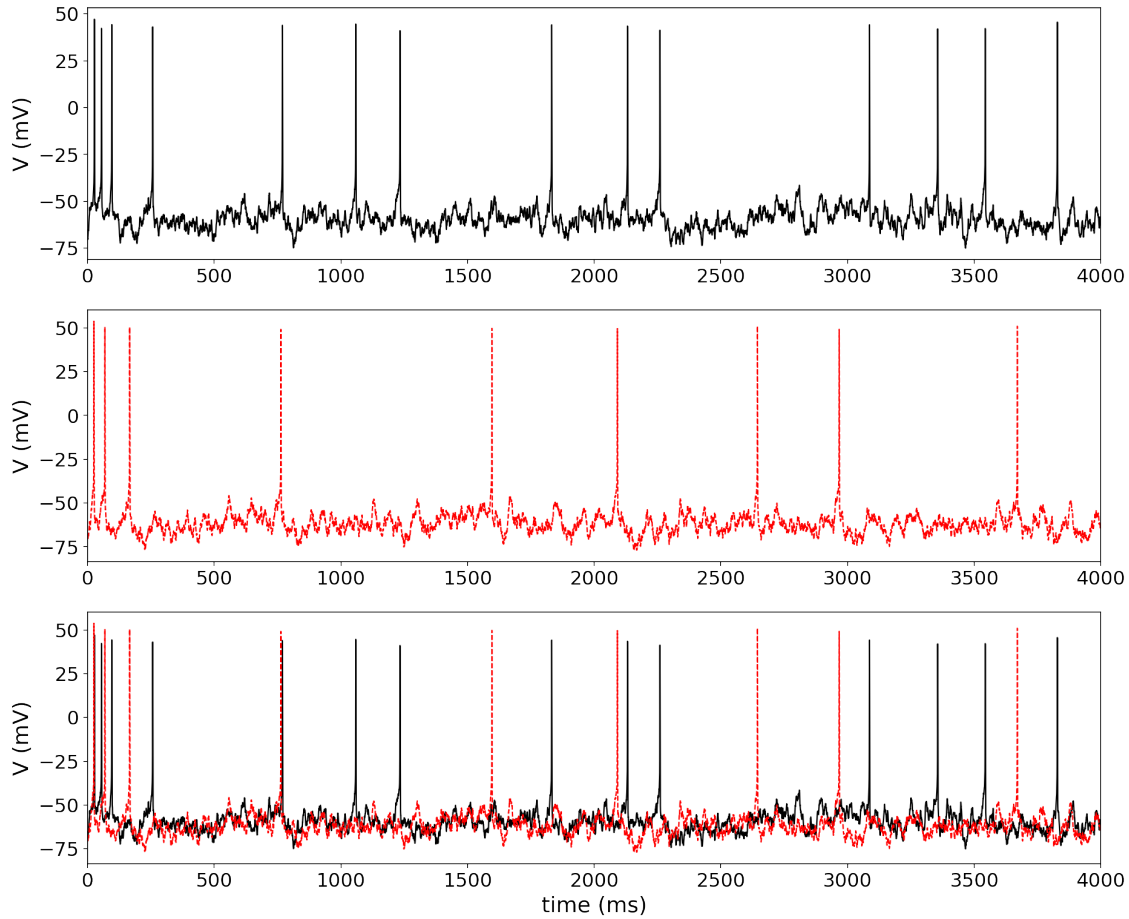
Figure 7: Responses of yPC (solid black traces) and aPC (dashed red traces) models to LFP forcing while in adaptive firing mode. Top panel shows just the yPC response, the second panel shows the aPC response, and the third panel shows the overlap of the two traces. Parameters for yPC and aPC models same as in Fig. 1. LFP parameters: μ_F=50.0 pA, σ_F=25.0 pA, τ_F=1/2.0 for both models.

boundaries for each firing pattern. The flexibility of the model could be useful for researchers looking to understand the effects of PC heterogeneity on network function. Geiller and colleagues [126] write, "Until very recently, hippocampus models and theories were built on a view of homogenous population of principal cells" (pg. 6). However, studies have shown that there is substantial heterogeneity in the firing patterns of CA1 PCs, especially during different development stages (for review, see [49]). Lee and colleagues [127] write, "how the heterogeneous PCs integrate into the CA1 circuit remains unknown" (pg. 1129).

Experimentally, it is difficult to precisely quantify how many PCs in a given network are displaying a specific firing pattern, and even harder if not impossible to manipulate these percentages. Furthermore, cells can transition between firing patterns [128], meaning the percentages might fluctuate. With our minimal model, however, we could build small networks with different balances of adapting versus bursting PCs, for example, and explore how changing these balances affects network output. We could also model the progression of aging in the network by varying the percentage of PCs which have altered Ca^{2+} channel density, or implement a whole spectrum of
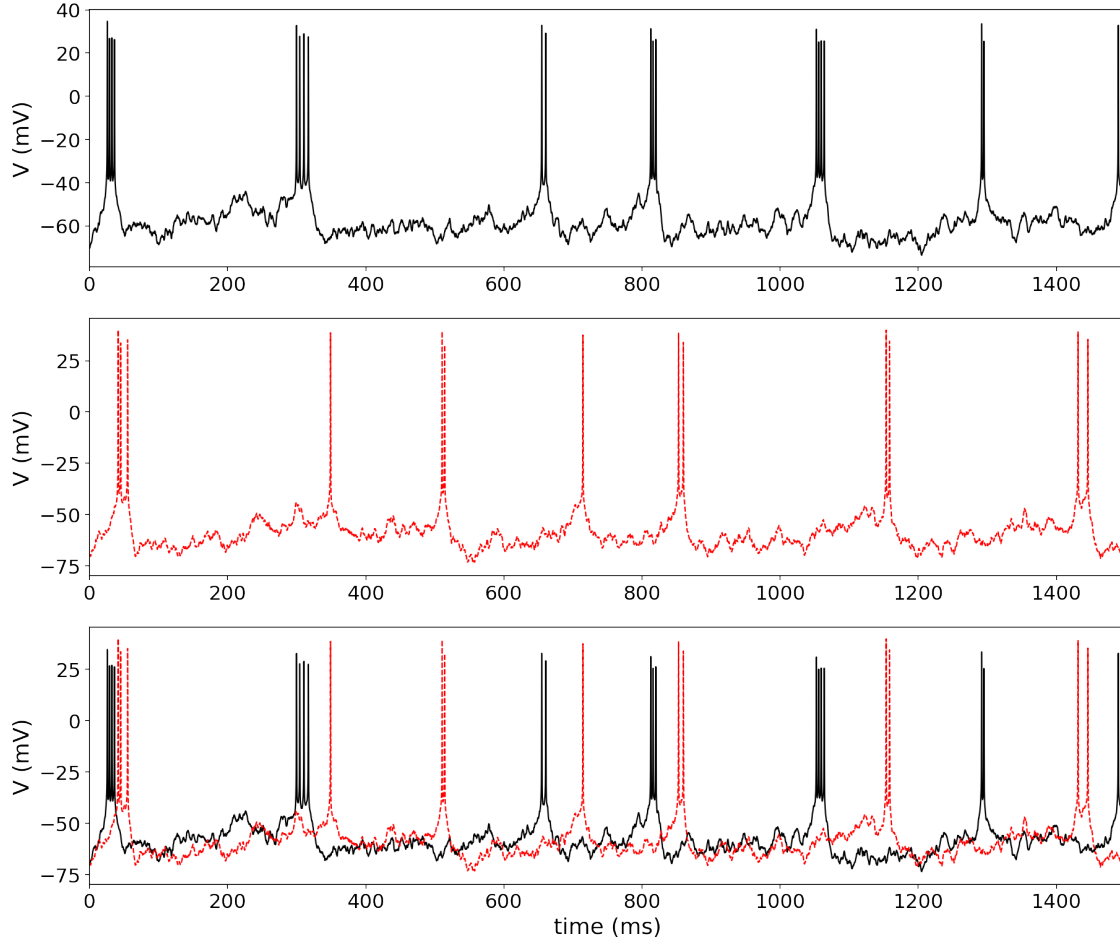
Figure 8: Responses of the conditionally bursting yPC (solid black traces) and aPC (dashed red traces) models to LFP forcing. Top panel shows just the yPC model response, the second panel shows the aPC response, and the third panel shows the overlap of the two traces. Parameters for yPC and aPC models are the same as in Fig. 4. LFP parameters the same as in Fig. 7 except σ_F=20.0 pA.

channel expression across the simulated network.

4.2   Aging and Ca^{2+} channel expression

Our model can also reproduce several changes in electrical activity observed in aged CA1 PCs, including larger AHPs [18–22] and increased adaptation [25–27]. We show that an increase in the L-type Ca^{2+} current amplitude to a level similar to that recorded in aged PCs is sufficient to reproduce the characteristic changes in cellular excitability associated with aging. The L-type channel in our study was modeled after the Ca$_v$1.2 isoform based on work which implicates this channel as the primary contributor in rodent brain, responsible for ~70-80% of the L-type current [70, 129]. mRNA expression of *Cacnac1C* (the gene encoding Ca$_v$1.2) is increased in aged mice and rats [31, 130]. Increases in plasma membrane expression [35] and phosphorylation [131] of Ca$_v$1.2 channels, both of which could lead to an increase in the number of 'functionally available' channels, have also been observed in aged rats. In addition, changes in *Cacna1c*/Ca$_v$1.2

367 expression are correlated with memory impairments [130, 132].

368 However, CA1 PCs also express the $Ca_v1.3$ isoform [133], which is responsible for $\sim$20% of
369 the total L-type current [70, 129]. Studies have found both increased mRNA [31] and protein
370 [33] expression of $Ca_v1.3$ in aged rats, and this increased expression is correlated with memory
371 impairment [34]. Knockout studies in mice indicate it is this isoform, and not $Ca_v1.2$, which
372 contributes to slow AHP generation [134], possibly via activation of colocalized SK channels [133].
373 While experimental studies have been complicated by a lack of pharmacological agents which can
374 isolate currents carried by the different isoforms, it would be relatively simple with our model to
375 study the contributions of these two channels. The primary difference between the two is a shift in
376 the activation curve of the $Ca_v1.3$ channel to more hyperpolarized values, relative to $Ca_v1.2$, with
377 half-activation potentials of around -20mV versus +3mV, respectively [87]. In the model, changing
378 the parameter v_j in Eq. 4 would allow us to represent the different isoforms to explore how changes
379 in the expression of each during aging might affect PC excitability.

380 Of course, there are many cellular changes apart from Ca^{2+} channel expression that occur during
381 aging and could contribute to altered electrical activity in PCs. For example, several studies
382 have implicated Ca^{2+} release from intracellular stores as an important contributor, particularly
383 to larger AHPs in aged animals [25, 110] (for reviews see [135, 136]). We did not explore the
384 role of intracellular Ca^{2+} stores in this study, nor many of the other cellular changes that surely
385 contribute to the multifactorial process of aging. It is not our intention to suggest that altered Ca^{2+}
386 channel expression is *the* factor altering the excitability of PCs in aged animals; it may not even
387 be the most important factor. We simply demonstrate that an increase in L-type Ca^{2+} channels is
388 *sufficient* to reproduce many of the changes in PC firing seen during aging. In addition, while some
389 of the modeling results we report here may hold experimentally at the cellular level (i.e., *in vitro*
390 or *in situ*), very different effects may be seen in the intact animal (i.e., *in vivo*) where all neuronal,
391 circuit-level interactions are preserved. It is known that the brain can compensate in a myriad of
392 ways for changes in cellular excitability and gene expression [137, 138], and these compensatory
393 mechanisms may work differently *in vivo* versus *in vitro* [139, 140].

4.3   Aging and excitability

395 Our simulations do show changes in the electrical activity of aged PCs, but do these changes
396 represent decreased excitability? This question relates more broadly to how we think about
397 excitability – the term is rarely clearly defined or used in a standardized way. In some studies,
398 excitability is used to refer to change in firing rate of a cell over the course of an injected current
399 pulse, claiming that PCs with stronger adaptation are less excitable (e.g., [26, 141]). In our
400 simulations under the adaptive firing parameter regime, the aPC model did have stronger adaptation
401 and fired fewer times during the stimulation period than the yPC model. However, under some
402 circumstances, this stronger adaptation occurred only after the aPC model cell initially fired
403 faster than the yPC model (see for example Fig. 3 inset). Should we consider this decreased
404 excitability?

405 If what concerns us with excitability is the activity of the cell over a given time period, then the
406 results under the bursting parameter regimes are even less clear. The aPC model always fired
407 fewer APs per burst than the yPC, indicating something akin to stronger adaptation. However, if

the 'event' we are considering is instead the burst, there are conditions under which aPCs fired a greater number of bursts in a given time period than yPCs. How should we interpret these results with respect to excitability? To our knowledge, there are very few experimental studies to date that have compared burst firing in young versus aged animal PCs, perhaps because of the relatively low percentage of cells with this firing pattern in certain developmental periods [118]. The only study of this type of which we are aware compared spontaneous burst firing in young versus aged animal PCs during rest and exploratory behavior [142]. Unfortunately, there are several factors that make it difficult to compare our results with theirs. First, their recordings were extracellular. As such, no bursts from individual PCs are shown in the paper to compare to our simulations, which reproduce intracellular firing patterns. Furthermore, the study focused on interspike intervals (ISIs), rather than the overall bursting pattern (e.g. number of bursts in a given period), which was our focus. Interestingly, Smith and colleagues [142] found that while ISIs were more left-skewed in aged animals when burst firing was recorded at rest, they found no difference between the age groups during behavior, suggesting that compensatory mechanisms work differently during behavior to adjust for changes in cellular excitability. Such compensatory mechanisms could be explored using our model, for example by adding simulated cholinergic input.

Returning to the idea of excitability, other researchers use the term to refer to how easy it is to get a cell to fire in response to stimulation. For example, Daoudal and colleagues [143] write, "Excitability can be defined as a propensity of the neuron to generate, beyond a certain threshold, an output signal – the action potential (AP) – from a given input signal..." (pg. 457). Similarly, Konstantinović and Filipović [144] write, "Neuronal excitability can be defined...as the readiness of a nerve cell or a neural circuit to respond to a stimulus" (pg. 234). In this context, excitability could be measured by the rheobase, or minimum current which generates firing in a neuron, as done in some studies of aging in CA1 (e.g., [145]). However, 'propensity' or 'readiness' could also be interpreted as how quickly a cell fires after stimulus onset. In the AHP simulations, we saw that the aPC model required 30 pA of additional current to fire the same number of spikes as for the yPC model. On the other hand, the aPC model often fired sooner than the yPC model and with larger amplitude APs in response to the same stimulus. These effects were a result of the increased Ca^{2+} channel density in aged cells – the larger Ca^{2+} current depolarized the cells faster and caused them to fire sooner, but it also caused the Ca^{2+}-dependent SK current to be larger and consequently slowed firing. It is as if the aPCs were initially more excitable, but then 'burned out' more quickly than the yPCs.

Overall, we believe our results highlight the importance of moving away from vague, ill-defined terms like 'excitability' in favor of clearer, more precise language that describes the effect of interest (e.g., PCs spiked faster, spiked sooner, etc.). We hope in a broader sense our study will encourage neuroscientists, and particularly aging researchers, to reevaluate how they think and write about excitability.

Funding

References

[1] M.M. Oh, F.A. Oliveira, and J.F. Disterhoft. Learning and aging related changes in intrinsic neuronal excitability. *Frontiers in Aging Neuroscience*, 2:2, 2010. https://doi.org/10.3389/neuro.24.002.2010.

[2] V. Rizzo, J. Richman, and S.V. Puthanveettil. Dissecting mechanisms of brain aging by studying the intrinsic excitability of neurons. *Frontiers in Aging Neuroscience*, 6:337, 2015. https://doi.org/10.3389/fnagi.2014.00337.

[3] E.S. Rosenzweig and C.A. Barnes. Impact of aging on hippocampal function: plasticity, network dynamics, and cognition. *Progress in Neurobiology*, 69(3):143–179, 2003. https://doi.org/10.1016/S0301-0082(02)00126-0.

[4] A.M. Fjell, L. McEvoy, D. Holland, A.M. Dale, K.B. Walhovd, and for the Alzheimer's Disease Neuroimaging Initiative. What is normal in normal aging? Effects of aging, amyloid and Alzheimer's disease on the cerebral cortex and the hippocampus. *Progress in Neurobiology*, 117:20–40, 2014. https://doi.org/10.1016/j.pneurobio.2014.02.004.

[5] M. Rodriguez, C. Rodriguez-Sabate, I. Morales, A. Sanchez, and M. Sabate. Parkinson's disease as a result of aging. *Aging Cell*, 14(3):293–308, 2015. https://doi.org/10.1111/acel.12312.

[6] C.A. Barnes. Memory deficits associated with senescence: A neurophysiological and behavioral study in the rat. *Journal of Comparative and Physiological Psychology*, 93(1):74–104, 1979. https://doi.org/10.1037/h0077579.

[7] C.A. Barnes and B.L. McNaughton. An age comparison of the rates of acquisition and forgetting of spatial information in relation to long-term enhancement of hippocampal synapses. *Behavioral Neuroscience*, 99(6):1040, 1985. https://doi.org/10.1037/0735-7044.99.6.1040.

[8] C.A. Barnes, G. Rao, and J. Shen. Age-related decrease in the N-methyl-D-aspartate R-mediated excitatory postsynaptic potential in hippocampal region CA1. *Neurobiology of Aging*, 18(4):445–452, 1997. https://doi.org/10.1016/S0197-4580(97)00044-4.

[9] F.H. Gage, S.B. Dunnett, and A. Björklund. Spatial learning and motor deficits in aged rats. *Neurobiology of Aging*, 5(1):43–48, 1984. https://doi.org/10.1016/0197-4580(84)90084-8.

[10] C.A. Barnes and B.L. McNaughton. Spatial memory and hippocampal synaptic plasticity in senescent and middle-aged rats. In D. Stein, editor, *The Psychobiology of Aging: Problems and Perspectives*, pages 253–272. Elsevier, 1980.

[11] A. Caprioli, O. Ghirardi, A. Giuliani, M.T. Ramacci, and L. Angelucci. Spatial learning and memory in the radial maze: A longitudinal study in rats from 4 to 25 months of age. *Neurobiology of Aging*, 12(5):605–607, 1991. https://doi.org/10.1016/0197-4580(91)90093-Y.

[12] M.C. Newman and A.W. Kaszniak. Spatial memory and aging: Performance on a human analog of the Morris water maze. *Aging, Neuropsychology, and Cognition*, 7(2):86–93, 2000. https://doi.org/10.1076/1382-5585(200006)7:2;1-U;FT086.

[13] S.M. Wilkniss, M.G. Jones, D.L. Korol, P.E. Gold, and C.A. Manning. Age-related differences in an ecologically based study of route learning. *Psychology and Aging*, 12(2):372, 1997. https://doi.org/10.1037/0882-7974.12.2.372.

[14] D.L. Deupree, J. Bradley, and D.A. Turner. Age-related alterations in potentiation in the CA1 region in F344 rats. *Neurobiology of Aging*, 14(3):249–258, 1993. https://doi.org/10.1016/0197-4580(93)90009-Z.

[15] E.S. Rosenzweig, G. Rao, B.L. McNaughton, and C.A. Barnes. Role of temporal summation in age-related long-term potentiation–induction deficits. *Hippocampus*, 7(5):549–558, 1997. https://doi.org/10.1002/(SICI)1098-1063(1997)7:5<549::AID-HIPO10>3.0.CO;2-0.

[16] P.W. Landfield and G. Lynch. Impaired monosynaptic potentiation in *in vitro* hippocampal slices from aged, memory-deficient rats. *Journal of Gerontology*, 32(5):523–533, 1977. https://doi.org/10.1093/geronj/32.5.523.

[17] P.W. Landfield, J.L. McGaugh, and G. Lynch. Impaired synaptic potentiation processes in the hippocampus of aged, memory-deficient rats. *Brain Research*, 150(1):85–101, 1978. https://doi.org/10.1016/0006-8993(78)90655-8.

[18] A. Kumar and T.C. Foster. 17β-estradiol benzoate decreases the AHP amplitude in CA1 pyramidal neurons. *Journal of Neurophysiology*, 88(2):621–626, 2002. https://doi.org/10.1152/jn.2002.88.2.621.

[19] A. Kumar and T. Foster. Environmental enrichment decreases the afterhyperpolarization in senescent rats. *Brain Research*, 1130:103–107, 2007. https://doi.org/10.1016/j.brainres.2006.10.037.

[20] P.W. Landfield and T.A. Pitler. Prolonged Ca^{2+}-dependent afterhyperpolarizations in hippocampal neurons of aged rats. *Science*, 226(4678):1089–1092, 1984. https://doi.org/10.1126/science.6494926.

[21] J.C. Gant and O. Thibault. Action potential throughput in aged rat hippocampal neurons: regulation by selective forms of hyperpolarization. *Neurobiology of Aging*, 30(12):2053–2064, 2009. https://doi.org/10.1016/j.neurobiolaging.2008.02.006.

[22] J.M. Power, W.W. Wu, E. Sametsky, M.M. Oh, and J.F. Disterhoft. Age-related enhancement of the slow outward calcium-activated potassium current in hippocampal CA1 pyramidal neurons in vitro. *Journal of Neuroscience*, 22(16):7234–7243, 2002. https://doi.org/10.1523/JNEUROSCI.22-16-07234.2002.

[23] B.E. Alger and R.A. Nicoll. Epileptiform burst afterhyperolarization: Calcium-dependent potassium potential in hippocampal CA1 pyramidal cells. *Science*, 210(4474):1122–1124, 1980. https://doi.org/10.1126/science.7444438.

[24] J.R. Hotson and D.A. Prince. A calcium-activated hyperpolarization follows repetitive firing in hippocampal neurons. *Journal of Neurophysiology*, 43(2):409–419, 1980. https://doi.org/10.1152/jn.1980.43.2.409.

[25] J.C. Gant, M.M. Sama, P.W. Landfield, and O. Thibault. Early and simultaneous emergence of multiple hippocampal biomarkers of aging is mediated by Ca^{2+}-induced Ca^{2+} release. *Journal of Neuroscience*, 26(13):3482–3490, 2006. https://doi.org/10.1523/JNEUROSCI.4171-05.2006.

[26] J.R. Moyer, L.T. Thompson, J.P. Black, and J.F. Disterhoft. Nimodipine increases excitability of rabbit CA1 pyramidal neurons in an age- and concentration-dependent manner. *Journal of Neurophysiology*, 68(6):2100–2109, 1992. https://doi.org/10.1152/jn.1992.68.6.2100.

[27] G.C. Tombaugh, W.B. Rowe, and G.M. Rose. The slow afterhyperpolarization in hippocampal CA1 neurons covaries with spatial learning ability in aged Fisher 344 rats. *Journal of Neuroscience*, 25(10):2609–2616, 2005. https://doi.org/10.1523/JNEUROSCI.5023-04.2005.

[28] L.W. Campbell, S-Y. Hao, O. Thibault, E.M. Blalock, and P.W. Landfield. Aging changes in voltage-gated calcium currents in hippocampal CA1 neurons. *Journal of Neuroscience*, 16(19):6286–6295, 1996. https://doi.org/10.1523/JNEUROSCI.16-19-06286.1996.

[29] M. Tanabe, B.H. Gähwiler, and U. Gerber. L-Type Ca^{2+} channels mediate the slow Ca^{2+}-dependent afterhyperpolarization current in rat CA3 pyramidal cells in vitro. *Journal of Neurophysiology*, 80(5):2268–2273, 1998. https://doi.org/10.1152/jn.1998.80.5.2268.

[30] O. Thibault, R. Hadley, and P.W. Landfield. Elevated postsynaptic $[Ca^{2+}]_i$ and L-type calcium channel activity in aged hippocampal neurons: Relationship to impaired synaptic plasticity. *Journal of Neuroscience*, 21(24):9744–9756, 2001. https://doi.org/10.1523/JNEUROSCI.21-24-09744.2001.

[31] J.P. Herman, K-C. Chen, R. Booze, and P.W. Landfield. Up-regulation of α_{1D} Ca^{2+} channel subunit mRNA expression in the hippocampus of aged F344 rats. *Neurobiology of Aging*, 19(6):581–587, 1998. https://doi.org/10.1016/S0197-4580(98)00099-2.

[32] O. Thibault and P.W. Landfield. Increase in single L-type calcium channels in hippocampal neurons during aging. *Science*, 272(5264):1017–1020, 1996. https://doi.org/10.1126/science.272.5264.1017.

[33] L.M. Veng and M.D. Browning. Regionally selective alterations in expression of the α_{1D} subunit ($Ca_v1.3$) of L-type calcium channels in the hippocampus of aged rats. *Molecular Brain Research*, 107(2):120–127, 2002. https://doi.org/10.1016/S0169-328X(02)00453-9.

[34] L.M. Veng, M.H. Mesches, and M.D. Browning. Age-related working memory impairment is correlated with increases in the L-type calcium channel protein α_{1D} ($Ca_v1.3$) in area CA1 of the hippocampus and both are ameliorated by chronic nimodipine treatment. *Molecular Brain Research*, 110(2):193–202, 2003. https://doi.org/10.1016/S0169-328X(02)00643-5.

[35] F.L. Núñez-Santana, M.M. Oh, M.D. Antion, A. Lee, J.W. Hell, and J.F. Disterhoft. Surface L-type Ca^{2+} channel expression levels are increased in aged hippocampus. *Aging Cell*, 13(1):111–120, 2014. https://doi.org/10.1111/acel.12157.

[36] C.M. Norris, S. Halpain, and T.C. Foster. Reversal of age-related alterations in synaptic plasticity by blockade of L-type Ca^{2+} channels. *Journal of Neuroscience*, 18(9):3171–3179, 1998. https://doi.org/10.1523/JNEUROSCI.18-09-03171.1998.

[37] M. Sandin, S. Jasmin, and T.E. Levere. Aging and cognition: Facilitation of recent memory in aged nonhuman primates by nimodipine. *Neurobiology of Aging*, 11(5):573–575, 1990. https://doi.org/10.1016/0197-4580(90)90120-O.

[38] A. Scriabine, T. Schuurman, and J. Traber. Pharmacological basis for the use of nimodipine in central nervous system disorders. *The FASEB Journal*, 3(7):1799–1806, 1989. https://doi.org/10.1096/fasebj.3.7.2565839.

[39] D. Bianchi, A. Marasco, A. Limongiello, C. Marchetti, H. Marie, B. Tirozzi, and M. Migliore. On the mechanisms underlying the depolarization block in the spiking dynamics of CA1 pyramidal neurons. *Journal of Computational Neuroscience*, 33(2):207–225, 2012. https://doi.org/10.1007/s10827-012-0383-y.

[40] D. Golomb, C. Yue, and Y. Yaari. Contribution of persistent Na^+ current and M-type K^+ current to somatic bursting in CA1 pyramidal cells: combined experimental and modeling study. *Journal of Neurophysiology*, 96(4):1912–1926, 2006. https://doi.org/10.1152/jn.00205.2006.

[41] N. Gu, K. Vervaeke, H. Hu, and J.F. Storm. Kv7/KCNQ/M and HCN/h, but not $K_{Ca}2$/SK channels, contribute to the somatic medium after-hyperpolarization and excitability control in CA1 hippocampal pyramidal cells. *Journal of Physiology*, 566(3):689–715, 2005. https://doi.org/10.1113/jphysiol.2005.086835.

[42] P. Poirazi, T. Brannon, and B.W. Mel. Arithmetic of subthreshold synaptic summation in a model CA1 pyramidal cell. *Neuron*, 37(6):977–987, 2003. https://doi.org/10.1016/S0896-6273(03)00148-X.

[43] M.M. Shah, M. Migliore, I. Valencia, E.C. Cooper, and D.A. Brown. Functional significance of axonal kv7 channels in hippocampal pyramidal neurons. *Proceedings of the National Academy of Sciences*, 105(22):7869–7874, 2008. https://doi.org/10.1073/pnas.0802805105.

[44] L-R. Shao, R. Halvorsrud, L. Borg-Graham, and J.F. Storm. The role of BK-type Ca^{2+}-dependent K^+ channels in spike broadening during repetitive firing in rat hippocampal pyramidal cells. *Journal of Physiology*, 521(1):135–146, 1999. https://doi.org/10.1111/j.1469-7793.1999.00135.x.

[45] A.L. Hodgkin and A.F. Huxley. A quantitative description of membrane current and its application to conduction and excitation in nerve. *The Journal of Physiology*, 117(4):500–544, 1952. https://doi.org/10.1113/jphysiol.1952.sp004764.

[46] M.A. Herrera-Valdez. A thermodynamic description for physiological transmembrane transport [version 2; peer review: 2 approved]. *F1000Research*, 7, 2018. https://doi.org/10.12688/f1000research.16169.2.

[47] M.A. Herrera-Valdez. Membranes with the same ion channel populations but different excitabilities. *PLOS ONE*, 7(4):e34636, 2012. https://doi.org/10.1371/journal.pone.0034636.

[48] M.A. Herrera-Valdez, E.C. McKiernan, S.D. Berger, S. Ryglewski, C. Duch, and S. Crook. Relating ion channel expression, bifurcation structure, and diverse firing patterns in a model of an identified motor neuron. *Journal of Computational Neuroscience*, 34(2):211–229, 2013. https://doi.org/10.1007/s10827-012-0416-6.

[49] E.C. McKiernan and D.F. Marrone. CA1 pyramidal cells have diverse biophysical properties, affected by development, experience, and aging. *PeerJ*, 5:e3836, 2017. https://doi.org/10.7717/peerj.3836.

[50] J.L. Hindmarsh and R.M. Rose. A model of neuronal bursting using three coupled first order differential equations. *Proceedings of the Royal Society B*, 221(1222):87–102, 1984. https://doi.org/10.1098/rspb.1984.0024.

[51] E. Av-Ron, H. Parnas, and L.A. Segel. A basic biophysical model for bursting neurons. *Biological Cybernetics*, 69(1):87–95, 1993. https://doi.org/10.1007/BF00201411.

[52] M.A. Herrera-Valdez and J. Lega. Reduced models for the pacemaker dynamics of cardiac cells. *Journal of Theoretical Biology*, 270(1):164–176, 2011. https://doi.org/10.1016/j.jtbi.2010.09.042.

[53] J. Rinzel. Excitation dynamics: insights from simplified membrane models. *Federation Proceedings*, 44(15):2944–2946, 1985. PMID: 2415401.

[54] E. Av-Ron, H. Parnas, and L. A. Segel. A minimal biophysical model for an excitable and oscillatory neuron. *Biological Cybernetics*, 65(6):487–500, 1991. https://doi.org/10.1007/BF00204662.

[55] M.A. Herrera-Valdez. An equation for the biological transmembrane potential from basic bio-physical principles [version 1; peer review: 2 not approved]. *F1000Research*, 9:676, 2020. https://doi.org/10.12688/f1000research.24205.1.

[56] L. Groc, Z. Petanjek, B. Gustafsson, Y. Ben-Ari, E. Hanse, and R. Khazipov. *In vivo* blockade of neural activity alters dendritic development of neonatal CA1 pyramidal cells. *European Journal of Neuroscience*, 16(10):1931–1938, 2002. https://doi.org/10.1046/j.1460-9568.2002.02264.x.

[57] B. Hille. *Ion Channels of Excitable Membranes*. Sinauer Associates, Sunderland, Massachusetts, U.S.A, 3rd edition, 2001.

[58] M. Stocker. Ca^{2+}-activated K^+ channels: Molecular determinants and function of the SK family. *Nature Reviews Neuroscience*, 5:758–770, 2004. https://doi.org/10.1038/nrn1516.

[59] M.I. Kalinin and S.A. Kononogov. Boltzmann's constant, the energy meaning of temper-ature, and thermodynamic irreversibility. *Measurement Techniques*, 48(7):632–636, 2005. https://doi.org/10.1007/s11018-005-0195-9.

[60] M. Covarrubias, A. Wei, and L. Salkoff. Shaker, Shal, Shab, and Shaw expresss independent K^+-current systems. *Neuron*, 7(5):763–773, 1991. https://doi.org/10.1016/0896-6273(91)90279-9.

[61] S. Tsunoda and L. Salkoff. The major delayed rectifier in both Drosophila neurons and muscle is encoded by Shab. *Journal of Neuroscience*, 15(7):5209–5221, 1995. https://doi.org/10.1523/JNEUROSCI.15-07-05209.1995.

[62] B. Hirschberg, J. Maylie, J.P. Adelman, and N.V. Marrion. Gating properties of single SK channels in hippocampal CA1 pyramidal neurons. *Biophysical Journal*, 77(4):1905–1913, 1999. https://doi.org/10.1016/S0006-3495(99)77032-3.

[63] B. Hirschberg, J. Maylie, J.P. Adelman, and N.V. Marrion. Gating of recombinant small-conductance Ca-activated K^+ channels by calcium. *Journal of General Physiology*, 111(4):565–581, 1998. https://doi.org/10.1085/jgp.111.4.565.

[64] M. Rudolph and A. Destexhe. Characterization of subthreshold voltage fluctuations in neuronal mem-branes. *Neural Computation*, 15(11):2577–2618, 2003. https://doi.org/10.1162/089976603322385081.

[65] D.T. Gillespie. The mathematics of Brownian motion and Johnson noise. *American Journal of Physics*, 64(3):225–239, 1996. https://doi.org/10.1119/1.18210.

[66] D.T. Gillespie. Exact numerical simulation of the Ornstein-Uhlenbeck process and its integral. *Physical Review E*, 54(2):2084, 1996. https://doi.org/10.1103/PhysRevE.54.2084.

[67] M. Rudolph, Z. Piwkowska, M. Badoual, T. Bal, and A. Destexhe. A method to estimate synaptic conductances from membrane potential fluctuations. *Journal of Neurophysiology*, 91(6):2884–2896, 2004. https://doi.org/10.1152/jn.01223.2003.

[68] A. Destexhe, M. Badoual, Z. Piwkowska, T. Bal, and M. Rudolph. A novel method for characterizing synaptic noise in cortical neurons. *Neurocomputing*, 58:191–196, 2004. https://doi.org/10.1016/j.neucom.2004.01.042.

[69] H. Murakoshi and J.S. Trimmer. Identification of the Kv2.1 K$^+$ channel as a major component of the delayed rectifier K$^+$ current in rat hippocampal neurons. *Journal of Neuroscience*, 19(5):1728–1735, 1999. https://doi.org/10.1523/JNEUROSCI.19-05-01728.1999.

[70] J.W. Hell, R.E. Westenbroek, C. Warner, M.K. Ahlijanian, W. Prystay, M.M. Gilbert, T.P. Snutch, and W.A. Catterall. Identification and differential subcellular localization of the neuronal class C and class D L-type calcium channel alpha 1 subunits. *Journal of Cell Biology*, 123(4):949–962, 1993. https://doi.org/10.1083/jcb.123.4.949.

[71] M. Li, J.W. West, Y. Lai, T. Scheuer, and W.A. Catterall. Functional modulation of brain sodium channels by cAMP-dependent phosphorylation. *Neuron*, 8(6):1151–1159, 1992. https://doi.org/10.1016/0896-6273(92)90135-Z.

[72] D.A. Fadool and I.B. Levitan. Modulation of olfactory bulb neuron potassium current by tyrosine phosphorylation. *Journal of Neuroscience*, 18(16):6126–6137, 1998. https://doi.org/10.1523/JNEUROSCI.18-16-06126.1998.

[73] J.B. Greer, M.C. Schmale, and L.A. Fieber. Whole-transcriptome changes in gene expression accompany aging of sensory neurons in *Aplysia californica*. *BMC Genomics*, 19(1):529, 2018. https://doi.org/10.1186/s12864-018-4909-1.

[74] S.O.M. Ketelaars, J.A. Gorter, E.A. van Vliet, F.H. Lopes da Silva, and W.J. Wadman. Sodium currents in isolated rat CA1 pyramidal and dentate granule neurones in the post-status epilepticus model of epilepsy. *Neuroscience*, 105(1):109–120, 2001. https://doi.org/10.1016/S0306-4522(01)00176-2.

[75] P. Sah, A.J. Gibb, and P.W. Gage. The sodium current underlying action potentials in guinea pig hippocampal CA1 neurons. *Journal of General Physiology*, 91(3):373–398, 1988. https://doi.org/10.1085/jgp.91.3.373.

[76] D.P. Mohapatra, H. Misonou, P. Sheng-Jun, J.E. Held, D.J. Surmeier, and J.S. Trimmer. Regulation of intrinsic excitability in hippocampal neurons by activity-dependent modulation of the K$_V$2.1 potassium channel. *Channels*, 3(1):46–56, 2009. https://doi.org/10.4161/chan.3.1.7655.

[77] J. Scuvée-Moreau, A. Boland, A. Graulich, L. Van Overmeire, D. D'hoedt, F. Graulich-Lorge, E. Thomas, A. Abras, M. Stocker, J-F. Liégeois, and V. Seutin. Electrophysiological characterization of the SK channel blockers methyl-laudanosine and methyl-noscapine in cell lines and rat brain slices. *British Journal of Pharmacology*, 143(6):753–764, 2004. https://doi.org/10.1038/sj.bjp.0705979.

[78] K.S. Richards, K. Bommert, G. Szabo, and R. Miles. Differential expression of Na$^+$/K$^+$-ATPase α-subunits in mouse hippocampal interneurones and pyramidal cells. *The Journal of Physiology*, 585(2):491–505, 2007. https://doi.org/10.1113/jphysiol.2007.144733.

[79] D. Johnston and S. M-S. Wu. *Foundations of Cellular Neurophysiology*. MIT Press, 1995.

[80] L.P. Endresen, K. Hall, J.S. Høye, and J. Myrheim. A theory for the membrane potential of living cells. *European Biophysics Journal*, 29(2):90–103, 2000. https://doi.org/10.1007/s002490050254.

[81] P.D. Weer, D.C. Gadsby, and R.F. Rakowski. Voltage dependence of the Na-K pump. *Annual Review of Physiology*, 50(1):225–241, 1988. https://doi.org/10.1146/annurev.ph.50.030188.001301.

[82] B.C. Carter and B.P. Bean. Sodium entry during action potentials of mammalian neurons: incomplete inactivation and reduced metabolic efficiency in fast-spiking neurons. *Neuron*, 64(6):898–909, 2009. https://doi.org/10.1016/j.neuron.2009.12.011.

[83] M. Estacion, A. Gasser, S.D. Dib-Hajj, and S.G. Waxman. A sodium channel mutation linked to epilepsy increases ramp and persistent current of Nav1.3 and induces hyperexcitability in hippocampal neurons. *Experimental Neurology*, 224(2):362–368, 2010. https://doi.org/10.1016/j.expneurol.2010.04.012.

[84] S. Gasparini and J.C. Magee. Phosphorylation-dependent differences in the activation properties of distal and proximal dendritic Na$^+$ channels in rat CA1 hippocampal neurons. *The Journal of Physiology*, 541(3):665–672, 2002. https://doi.org/10.1113/jphysiol.2002.020503.

[85] M. Martina and P. Jonas. Functional differences in Na$^+$ channel gating between fast-spiking interneurones and principal neurones of rat hippocampus. *The Journal of Physiology*, 505(3):593–603, 1997. https://doi.org/10.1111/j.1469-7793.1997.593ba.x.

[86] J.C. Magee and D. Johnston. Characterization of single voltage-gated Na$^+$ and Ca^{2+} channels in apical dendrites of rat CA1 pyramidal neurons. *The Journal of Physiology*, 487(1):67, 1995. https://doi.org/10.1113/jphysiol.1995.sp020862.

[87] W. Xu and D. Lipscombe. Neuronal Ca$_v$1.3 α_1 L-type channels activate at relatively hyperpolarized membrane potentials and are incompletely inhibited by dihydropyridines. *Journal of Neuroscience*, 21(16):5944–5951, 2001. https://doi.org/10.1523/JNEUROSCI.21-16-05944.2001.

[88] B. Balasubramanian, J.P. Imredy, D. Kim, J. Penniman, A. Lagrutta, and J.J. Salata. Optimization of Ca$_v$1.2 screening with an automated planar patch clamp platform. *Journal of Pharmacological and Toxicological Methods*, 59(2):62–72, 2009. https://doi.org/10.1016/j.vascn.2009.02.002.

[89] B.C. Carter, A.J. Giessel, B.L. Sabatini, and B.P. Bean. Transient sodium current at subthreshold voltages: activation by epsp waveforms. *Neuron*, 75(6):1081–1093, 2012. http://dx.doi.org/10.1016/j.neuron.2012.08.033.

[90] P.F. Costa. The kinetic parameters of sodium currents in maturing acutely isolated rat hippocampal CA1 neurones. *Developmental Brain Research*, 91(1):29–40, 1996. https://doi.org/10.1016/0165-3806(95)00159-X.

[91] A.M.J. VanDongen, G.C. Frech, J.A. Drewe, R.H. Joho, and A.M. Brown. Alteration and restoration of K$^+$ channel function by deletions at the N-and C-termini. *Neuron*, 5(4):433–443, 1990. https://doi.org/10.1016/0896-6273(90)90082-Q.

[92] M.M. Oh, F.A. Oliveira, J. Waters, and J.F. Disterhoft. Altered calcium metabolism in aging CA1 hippocampal pyramidal neurons. *Journal of Neuroscience*, 33(18):7905–7911, 2013. https://doi.org/10.1523/JNEUROSCI.5457-12.2013.

[93] J.C. Magee, R.B. Avery, B.R. Christie, and D. Johnston. Dihydropyridine-sensitive, voltage-gated Ca^{2+} channels contribute to the resting intracellular Ca^{2+} concentration of hippocampal CA1 pyramidal neurons. *Journal of Neurophysiology*, 76(5):3460–3470, 1996. https://doi.org/10.1152/jn.1996.76.5.3460.

[94] C.R. Harris, K.J. Millman, S.J. van der Walt, R. Gommers, P. Virtanen, D. Cournapeau, E. Wieser, J. Taylor, S. Berg, N.J. Smith, R. Kern, M. Picus, S. Hoyer, M.H. van Kerkwijk, M. Brett, A. Haldane, J. Fernández del Río, M. Wiebe, P. Peterson, P. Gérard-Marchant, K. Sheppard, T. Reddy,

W. Weckesser, H. Abbasi, C. Gohlke, and T.E. Oliphant. Array programming with NumPy. *Nature*, 585(7825):357–362, 2020. https://doi.org/10.1038/s41586-020-2649-2.

[95] J.D. Hunter. Matplotlib: A 2D graphics environment. *Computing in Science & Engineering*, 9(3):90–95, 2007. https://doi.org/10.1109/MCSE.2007.55.

[96] D. Mondaca. pyprocess, 2012–. https://github.com/Zincr0/pyprocess.

[97] F. Pérez and B.E. Granger. IPython: a system for interactive scientific computing. *Computing in Science & Engineering*, 9(3):21–29, 2007. https://doi.org/10.1109/MCSE.2007.53.

[98] T. Kluyver, B. Ragan-Kelley, F. Pérez, B.E. Granger, M. Bussonnier, J. Frederic, K. Kelley, J.B. Hamrick, J. Grout, S. Corlay, P. Ivanov, D. Avila, S. Abdalla, C. Willing, and Jupyter Development Team. Jupyter Notebooks-a publishing format for reproducible computational workflows. In F. Loizides and B. Schmidt, editors, *Positioning and Power in Academic Publishing: Players, Agents and Agendas*, pages 87–90, 2016. https://doi.org/10.3233/978-1-61499-649-1-87.

[99] K.C. Chen, E.M. Blalock, O. Thibault, P. Kaminker, and P.W. Landfield. Expression of α1D subunit mRNA is correlated with L-type Ca^{2+} channel activity in single neurons of hippocampal "zipper" slices. *Proceedings of the National Academy of Sciences*, 97(8):4357–4362, 2000. https://doi.org/10.1073/pnas.070056097.

[100] D.V. Madison and R.A. Nicoll. Control of the repetitive discharge of rat CA1 pyramidal neurones in vitro. *Journal of Physiology*, 354(1):319–331, 1984. https://doi.org/10.1113/jphysiol.1984.sp015378.

[101] R.W. Stackman, R.S. Hammond, E. Linardatos, A. Gerlach, J. Maylie, J.P. Adelman, and T. Tzounopoulos. Small conductance Ca^{2+}-activated K^+ channels modulate synaptic plasticity and memory encoding. *Journal of Neuroscience*, 22(23):10163–10171, 2002. https://doi.org/10.1523/JNEUROSCI.22-23-10163.2002.

[102] M. Borde, J.R. Cazalets, and W. Buno. Activity-dependent response depression in rat hippocampal CA1 pyramidal neurons in vitro. *Journal of Neurophysiology*, 74(4):1714–1729, 1995. https://doi.org/10.1152/jn.1995.74.4.1714.

[103] N. Gu, H. Hu, K. Vervaeke, and J.F. Storm. SK ($K_{Ca}2$) channels do not control somatic excitability in CA1 pyramidal neurons but can be activated by dendritic excitatory synapses and regulate their impact. *Journal of Neurophysiology*, 100(5):2589–2604, 2008. https://doi.org/10.1152/jn.90433.2008.

[104] S-C. Jung and D.A. Hoffman. Biphasic somatic A-type K+ channel downregulation mediates intrinsic plasticity in hippocampal CA1 pyramidal neurons. *PLOS ONE*, 4(8):e6549, 2009. https://doi.org/10.1371/journal.pone.0006549.

[105] J. Kim, D-S. Wei, and D.A. Hoffman. Kv4 potassium channel subunits control action potential repolarization and frequency-dependent broadening in rat hippocampal CA1 pyramidal neurones. *Journal of Physiology*, 569(1):41–57, 2005. https://doi.org/10.1113/jphysiol.2005.095042.

[106] R. Malik and S. Chattarji. Enhanced intrinsic excitability and EPSP-spike coupling accompany enriched environment-induced facilitation of LTP in hippocampal CA1 pyramidal neurons. *Journal of Neurophysiology*, 107(5):1366–1378, 2012. https://doi.org/10.1152/jn.01009.2011.

[107] J.F. Disterhoft, L.T. Thompson, J.R. Moyer, and D.J. Mogul. Calcium-dependent afterhyperpo-larization and learning in young and aging hippocampus. *Life Sciences*, 59(5):413–420, 1996. https://doi.org/10.1016/0024-3205(96)00320-7.

[108] J.F. Storm. An after-hyperpolarization of medium duration in rat hippocampal pyramidal cells. *Journal of Physiology*, 409(1):171–190, 1989. https://doi.org/10.1113/jphysiol.1989.sp017491.

[109] J.F. Storm. Potassium currents in hippocampal pyramidal cells. *Progress in Brain Research*, 83:161–187, 1990. https://doi.org/10.1016/S0079-6123(08)61248-0.

[110] K. Bodhinathan, A. Kumar, and T.C. Foster. Redox sensitive calcium stores underlie enhanced after hyperpolarization of aged neurons: role for ryanodine receptor mediated calcium signaling. *Journal of Neurophysiology*, 104(5):2586–2593, 2010. https://doi.org/10.1152/jn.00577.2010.

[111] E.M. Blalock, J.T. Phelps, T. Pancani, J.L. Searcy, K.L. Anderson, J.C. Gant, J. Popovic, M.G. Avdiushko, D.A. Cohen, K.-C. Chen, N.M. Porter, and O. Thibault. Effects of long-term piogli-tazone treatment on peripheral and central markers of aging. *PLOS ONE*, 5(4):e10405, 2010. https://doi.org/10.1371/journal.pone.0010405.

[112] C.C. Kaczorowski and J.F. Disterhoft. Memory deficits are associated with impaired ability to modulate neuronal excitability in middle-aged mice. *Learning & Memory*, 16(6):362–366, 2009. https://doi.org/10.1101/lm.1365609.

[113] E.A. Matthews, J.M. Linardakis, and J.F. Disterhoft. The fast and slow afterhyperpolarizations are differentially modulated in hippocampal neurons by aging and learning. *Journal of Neuroscience*, 29(15):4750–4755, 2009. https://doi.org/10.1523/JNEUROSCI.0384-09.2009.

[114] C.C. Kaczorowski, J. Disterhoft, and N. Spruston. Stability and plasticity of intrinsic membrane properties in hippocampal ca1 pyramidal neurons: effects of internal anions. *The Journal of Physiology*, 578(3):799–818, 2007. https://doi.org/10.1113/jphysiol.2006.124586.

[115] R. Azouz, M.S. Jensen, and Y. Yaari. Ionic basis of spike after-depolarization and burst genera-tion in adult rat hippocampal CA1 pyramidal cells. *Journal of Physiology*, 492(1):211–223, 1996. https://doi.org/10.1113/jphysiol.1996.sp021302.

[116] M.S. Jensen, R. Azouz, and Y. Yaari. Variant firing patterns in rat hippocampal pyramidal cells modulated by extracellular potassium. *Journal of Neurophysiology*, 71(3):831–839, 1994. https://doi.org/10.1152/jn.1994.71.3.831.

[117] H. Su, G. Alroy, E.D. Kirson, and Y. Yaari. Extracellular calcium modulates persistent sodium current-dependent burst-firing in hippocampal pyramidal neurons. *Journal of Neuroscience*, 21(12):4173–4182, 2001. https://doi.org/10.1523/JNEUROSCI.21-12-04173.2001.

[118] S. Chen, C. Yue, and Y. Yaari. A transitional period of Ca^{2+}-dependent spike afterdepolarization and bursting in developing rat CA1 pyramidal cells. *Journal of Physiology*, 567(1):79–93, 2005. https://doi.org/10.1113/jphysiol.2005.084590.

[119] M.S. Jensen, R. Azouz, and Y. Yaari. Spike after-depolarization and burst generation in adult rat hippocampal CA1 pyramidal cells. *The Journal of Physiology*, 492(1):199–210, 1996. https://doi.org/10.1113/jphysiol.1996.sp021301.

[120] F. Manseau and S. Williams. Tuning in the hippocampal theta band in vitro: methodologies for recording from the isolated rodent septohippocampal circuit. *Journal of Visualized Experiments*, 126:e55851, 2017. https://doi.org/10.3791/55851.

[121] Q. Yang, Y-D. Hu, X-F. Wang, and F-S. Zheng. Dl-3n-butylphthalide reduces epileptiform activity through GluA2-lacking calcium-permeable AMPARs in epilepsy models. *Oncotarget*, 8(58):98242, 2017. https://doi.org/10.18632/oncotarget.21529.

[122] B.H. Bland, J. Konopacki, and R.H. Dyck. Relationship between membrane potential oscillations and rhythmic discharges in identified hippocampal theta-related cells. *Journal of Neurophysiology*, 88(6):3046–3066, 2002. https://doi.org/10.1152/jn.00315.2002.

[123] B.H. Bland, J. Konopacki, and R. Dyck. Heterogeneity among hippocampal pyramidal neurons revealed by their relation to theta-band oscillation and synchrony. *Experimental Neurology*, 195(2):458–474, 2005. https://doi.org/10.1016/j.expneurol.2005.06.007.

[124] C.Y.L. Huh, B. Amilhon, K.A. Ferguson, F. Manseau, S.G. Torres-Platas, J.P. Peach, S. Scodras, N. Mechawar, F.K. Skinner, and S. Williams. Excitatory inputs determine phase-locking strength and spike-timing of CA1 stratum oriens/alveus parvalbumin and somatostatin interneurons during intrinsically generated hippocampal theta rhythm. *Journal of Neuroscience*, 36(25):6605–6622, 2016. https://doi.org/10.1523/JNEUROSCI.3951-13.2016.

[125] L.V. Colom and B.H. Bland. State-dependent spike train dynamics of hippocampal formation neurons: evidence for theta-on and theta-off cells. *Brain Research*, 422(2):277–286, 1987. https://doi.org/10.1016/0006-8993(87)90934-6.

[126] T. Geiller, S. Royer, and J-S. Choi. Segregated cell populations enable distinct parallel encoding within the radial axis of the CA1 pyramidal layer. *Experimental Neurobiology*, 26(1):1–10, 2017. https://doi.org/10.5607/en.2017.26.1.1.

[127] S-H. Lee, I. Marchionni, M. Bezaire, C. Varga, N. Danielson, M. Lovett-Barron, A. Losonczy, and I. Soltesz. Parvalbumin-positive basket cells differentiate among hippocampal pyramidal cells. *Neuron*, 82(5):1129–1144, 2014. https://doi.org/10.1016/j.neuron.2014.03.034.

[128] M. Steriade, I. Timofeev, N. Dürmüller, and F. Grenier. Dynamic properties of corticothalamic neurons and local cortical interneurons generating fast rhythmic (30–40 Hz) spike bursts. *Journal of Neurophysiology*, 79(1):483–490, 1998. https://doi.org/10.1152/jn.1998.79.1.483.

[129] M.J. Sinnegger-Brauns, A. Hetzenauer, I.G. Huber, E. Renström, G. Wietzorrek, S. Berjukov, M. Cavalli, D. Walter, A. Koschak, R. Waldschütz, S. Herin, S. Bova, P. Rorsman, O. Pongs, N. Singewald, and J. Striessnig. Isoform-specific regulation of mood behavior and pancreatic β cell and cardiovascular function by L-type Ca^{2+} channels. *The Journal of Clinical Investigation*, 113(10):1430–1439, 2004. https://doi.org/10.1172/JCI20208.

[130] P. Zanos, S. Bhat, C.E. Terrillion, R.J. Smith, L.H. Tonelli, and T.D. Gould. Sex-dependent modulation of age-related cognitive decline by the L-type calcium channel gene *Cacna1c* (Ca_v1.2). *European Journal of Neuroscience*, 42(8):2499–2507, 2015. https://doi.org/10.1111/ejn.12952.

[131] M.A. Davare and J.W. Hell. Increased phosphorylation of the neuronal L-type Ca^{2+} channel Ca_v1.2 during aging. *Proceedings of the National Academy of Sciences*, 100(26):16018–16023, 2003. https://doi.org/10.1073/pnas.2236970100.

[132] S. Moosmang, N. Haider, N. Klugbauer, H. Adelsberger, N. Langwieser, J. Müller, M. Stiess, E. Marais, V. Schulla, L. Lacinova, S. Goebbels, K.A. Nave, D.R. Storm, F. Hofmann, and T. Kleppisch. Role of hippocampal Ca$_v$1.2 Ca^{2+} channels in NMDA receptor-independent synaptic plasticity and spatial memory. *Journal of Neuroscience*, 25(43):9883–9892, 2005. https://doi.org/10.1523/JNEUROSCI.1531-05.2005.

[133] S.E.H. Bowden, S. Fletcher, D.J. Loane, and N.V. Marrion. Somatic colocalization of rat SK1 and D class (Ca$_v$1.2) L-type calcium channels in rat CA1 hippocampal pyramidal neurons. *Journal of Neuroscience*, 21(20):RC175–RC175, 2001. https://doi.org/10.1523/JNEUROSCI.21-20-j0006.2001.

[134] A.E. Gamelli, B.C. McKinney, J.A. White, and G.G. Murphy. Deletion of the L-type calcium channel Ca$_v$1.3 but not Ca$_v$1.2 results in a diminished sAHP in mouse CA1 pyramidal neurons. *Hippocampus*, 21(2):133–141, 2011. https://doi.org/10.1002/hipo.20728.

[135] O. Thibault, J.C. Gant, and P.W. Landfield. Expansion of the calcium hypothesis of brain aging and Alzheimer's disease: minding the store. *Aging Cell*, 6(3):307–317, 2007. https://doi.org/10.1111/j.1474-9726.2007.00295.x.

[136] E.C. Toescu and M. Vreugdenhil. Calcium and normal brain ageing. *Cell Calcium*, 47(2):158–164, 2010. https://doi.org/10.1016/j.ceca.2009.11.013.

[137] R. Grashow, T. Brookings, and E. Marder. Compensation for variable intrinsic neuronal excitability by circuit-synaptic interactions. *Journal of Neuroscience*, 30(27):9145–9156, 2010. https://doi.org/10.1523/JNEUROSCI.0980-10.2010.

[138] E.Z. Kim, J. Vienne, M. Rosbash, and L.C. Griffith. Nonreciprocal homeostatic compensation in drosophila potassium channel mutants. *Journal of Neurophysiology*, 117(6):2125–2136, 2017. https://doi.org/10.1152/jn.00002.2017.

[139] J. Echegoyen, A. Neu, K.D. Graber, and I. Soltesz. Homeostatic plasticity studied using in vivo hippocampal activity-blockade: synaptic scaling, intrinsic plasticity and age-dependence. *PLOS ONE*, 2(8):e700, 2007. https://doi.org/10.1371/journal.pone.0000700.

[140] P.J. Morgan, R. Bourboulou, C. Filippi, J. Koenig-Gambini, and J. Epsztein. Kv1.1 contributes to a rapid homeostatic plasticity of intrinsic excitability in CA1 pyramidal neurons in vivo. *eLife*, 8:e49915, 2019. https://doi.org/10.7554/eLife.49915.

[141] M.M. Oh, J.M. Power, L.T. Thompson, P.L. Moriearty, and J.F. Disterhoft. Metrifonate increases neuronal excitability in CA1 pyramidal neurons from both young and aging rabbit hippocampus. *Journal of Neuroscience*, 19(5):1814–1823, 1999. https://doi.org/10.1523/JNEUROSCI.19-05-01814.1999.

[142] A.C. Smith, J.L. Gerrard, C.A. Barnes, and B.L. McNaughton. Effect of age on burst firing characteristics of rat hippocampal pyramidal cells. *NeuroReport*, 11(17):3865–3871, 2000. https://doi.org/10.1097/00001756-200011270-00052.

[143] G. Daoudal and D. Debanne. Long-term plasticity of intrinsic excitability: learning rules and mechanisms. *Learning & Memory*, 10(6):456–465, 2003. https://doi.org/10.1101/lm.64103.

[144] L.M. Konstantinović and S.R. Filipović. Effects of near-infrared low-level laser stimulation on neuronal excitability. In M.R. Hamblin and Y-Y. Huang, editors, *Photobiomodulation in the Brain: Low-Level Laser (Light) Therapy in Neurology and Neuroscience*, pages 233–240. Academic Press, 2019. https://doi.org/10.1016/B978-0-12-815305-5.00018-X.

[145] B. Potier, Y. Lamour, and P. Dutar. Age-related alterations in the properties of hippocampal pyramidal neurons among rat strains. *Neurobiology of Aging*, 14(1):17–25, 1993. https://doi.org/10.1016/0197-4580(93)90016-5.